ACS OMEGA

Open Access

This article is licensed under CC-BY-NC-ND 4.0

http://pubs.acs.org/journal/acsodf

Article

Experimental and Computational Anticorrosion Behaviors of Pyrazole *s*-Triazine/anilino-morpholino Derivatives for Steel in Acidic Solutions

Hassan H. Hammud,* Waleed A. Aljamhi, Ihab Shawish, Nur Hazimah B. Z Arfan, Malai Haniti S. A. Hamid, Nadeem S. Sheikh,* Hany M. Abd El-Lateef,* Assem Barakat, and Ayman El-Faham

Cite This: *ACS Omega* 2024, 9, 31714−31731

Read Online

ACCESS | Metrics & More | Article Recommendations | Supporting Information

ABSTRACT: The corrosion inhibition of C-steel by two *s*-triazine/morpholino-anilino-pyrazole derivatives, namely, 4-(3,5-dimethyl-1*H*-pyrazol-1-yl)-6-morpholino-*N*-phenyl-1,3,5-triazin-2-amine (**1**) and *N*-(4-bromophenyl)-4-(3,5-dimethyl-1*H*-pyrazol-1-yl)-6-morpholino-1,3,5-triazin-2-amine (**2**) was investigated by impedimetric and potentiometric studies. It was found that (**1**) and (**2**) acted as cathodic-type corrosion inhibitors that retard the hydrogen evolution reaction. The percent corrosion inhibition, 98.5% for compound (**2**) (with bromo substituent) at 80 ppm, was slightly higher than 97.8% for (**1**) at 100 ppm. Thus, the replacement of a −H with −Br substituent increased the corrosion inhibition properties. Compound (**2**) exhibited Temkin isotherm adsorption, whereas compound (**1**) exhibited Langmuir adsorption. Scanning electron microscopy (SEM) analysis of the steel surface indicated that the inhibitors caused protection of the surface. The weight loss experiment also proved the decrease in the corrosion rate when inhibitors were added. The difference in inhibitory efficiency between compounds (**1**) and (**2**) was investigated by density functional theory (DFT) to study neutral and protonated species in gaseous and aqueous phases. The theoretical analysis demonstrated that compound (**2**) exhibited higher inhibitory activity on a metal surface compared to compound (**1**), aligning with the experimental results. The energy associated with the metal/adsorbate arrangement, represented by dE_{ads}/dN_i, was higher for (**2**) (−380.91 kcal mol^{-1}) compared to (**1**) (−371.64 kcal mol^{-1}). This indicated better adsorption of (**2**) over (**1**).

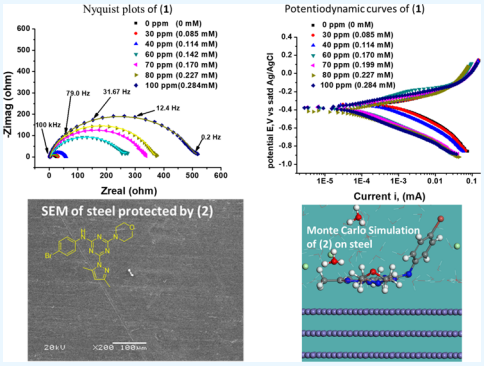

INTRODUCTION

C-steel is commonly used in buildings and infrastructure construction. Acid solutions such as hydrochloric acid HCl were commonly used in the chemical industry to remove the scales from metallic surfaces. However, the use of corrosive acid media for cleaning eventually causes the corrosion of metals. Current researchers focused on finding efficient inhibitors that can protect the iron surface from the corrosive effect of acids. The investigation of corrosion of steel exposed to an acidic medium has gained significant importance due to its widespread use in numerous industries for preservation, cleaning, descaling, etc.[1−6] Carbon steel is highly favored in industries due to its low cost, widespread availability, and exceptional mechanical strength. Effective corrosion control is crucial for both economic and environmental reasons. Consequently, there is a growing need to explore novel and efficient corrosion inhibitors to safeguard metals from corrosion.

In this context, organic inhibitors hold a prominent position among the corrosion inhibitors for steel due to their remarkable capacity to form a protective film on the steel's surface. Recently, several kinds of heterocyclic macrocyclic compounds and biomolecules and their various chemically modified derivatives and composites were reported as corrosion inhibitors.[7−9]

The effectiveness of these inhibitors depends on their electronic structure, chemical composition, the presence of specific functional groups, and their adsorption to the steel surface.[8−13] Recently, *s*-triazine derivatives have shown promising influence as corrosion inhibitors of carbon steel.[14] In fact, the development of such type of a corrosion inhibitor has assumed a paramount impact within the industrial sector. Typically, organic inhibitors function by forming a protective film on the surface of metal, preventing metal dissolution in an acid solution. Thus, the effectiveness of inhibition depends on

Received: March 16, 2024
Revised: June 7, 2024
Accepted: June 28, 2024
Published: July 11, 2024

ACS Publications

© 2024 The Authors. Published by American Chemical Society

https://doi.org/10.1021/acsomega.4c02569
ACS Omega 2024, 9, 31714−31731

the affinities exhibited by organic molecules toward the metal surface. This affinity is remarkably influenced by the inhibitor electronic structure, electron density, aromatic nature, and the presence of polar functional groups.[13,15−17]

Xuehui et al.[18] investigated the corrosion inhibitor activity of 2,4,6-tri(2-pyridyl)-*s*-triazine (TPT) toward mild steel in an HCl solution at room temperature. Scanning electron microscopy (SEM) analysis demonstrated that this *s*-triazine derivative had a protective effect on the metal. The protection was attributed to the formation of an adsorption coating film on the surface, which mitigated the aggressive corrosion process. Another study by Yoo et al.[19] investigated the corrosion-inhibiting behavior of s-triazine polycarboxylate hybrids. The results of the Langmuir isotherm model confirmed that the presence of the triazine ring significantly enhanced the rust-preventing characteristics. Later, Abd El-Lateef et al.[20] explored the performance of novel tetrahydro-1,2,4-triazines as corrosion inhibitors of N80 steel in a 5% sulfamic acid medium. The results of electrochemical data, Langmuir adsorption isotherm, and the negative values of ΔG_{ads}^{0} showed that the tested compounds were classified as mixed-type inhibitors with exceptional efficacy as corrosion inhibitors of N80 carbon steel metal. However, issues related to solubility often arise with triazine derivatives, leading to a considerable inhibition of their anticorrosive activity. Thereby, the incorporation of polar heterocyclic substituents like a morpholine group to the triazine core enhanced the corrosion-inhibiting activity of steel in an acidic medium.[21] Greco et al.[22] evaluated the corrosion inhibition of two newly developed *s*-triazine hybrid molecules incorporating a morpholine group on AISI 316 stainless steel. The results demonstrated that they exhibited remarkable efficacy in the formation of a protective film on the surface of the tested stainless samples with corrosion-inhibiting efficiency IE% = 77%. El-Faham et al.[23] explored the inhibitory effect of 2,4-dihydrazino-morpholino-1,3,5-triazines on the corrosion of steel in an HCl solution through electrochemical studies. The potentiodynamic polarization measurements demonstrated that they acted as mixed-type inhibitors and formed insulating layers on the surface of the steel, causing corrosion inhibition.

The inhibitory efficiency of a molecule on the metal surface could be assessed using sophisticated computational tools. It allows economical accessibility to valuable and crucial results in analyzing the affinities between the studied molecular inhibitor and its inhibition efficiency even for an architecturally complicated molecular structure.[24] Density functional theory (DFT) has been a widely utilized quantum mechanical method in the exploration of the quantum corrosion field,[25] as it allows the understanding of the reactivity behavior of the inhibitor and, thus, its mechanistic details.[26] The chemical reactivity is reportedly linked to the frontier molecular orbitals results obtained computationally.[27]

Owing to the crucial activity of *s*-triazine and morpholine motifs as corrosion inhibitors of steel in an acidic environment, herein, we investigated the corrosion inhibitor properties of recently synthesized derivatives. The structural skeleton of these molecules is based on an *s*-triazine scaffold bearing both morpholine and pyrazole motifs while including either an unsubstituted anilino group (**1**) or a bromoaniline group (**2**) (Figure 1).[28] This study encompassed a comprehensive electrochemical analysis complemented by density functional theory (DFT) data to explore the potential of these molecules as corrosion inhibitors of carbon steel in an acidic environment. Also, a theoretical investigation was carried out to predict its mechanism and its inhibitory efficiencies. Parameters like total electronic energy, dipole moment, highest occupied molecular orbital (HOMO) and lowest-unoccupied molecular orbital (LUMO) orbital energies, energy gap, electron affinity, ionization potential, hardness, softness, electronegativity, chemical potential, electrophilicity, fractions of electron transferred, and back-donation were calculated. In addition, Fukui indices have been employed to explore the local reactivity of the studied inhibitors.

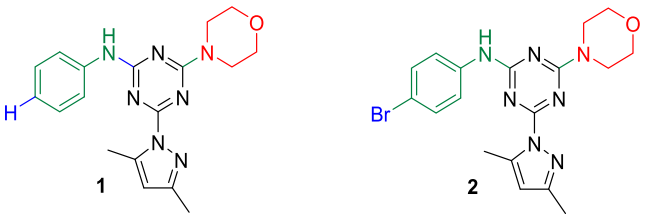

Figure 1. Molecular structure of unsubstituted (**1**) and bromine-substituted (**2**) *s*-triazine/anilino-morpholino molecules.

■ RESULTS AND DISCUSSION

Inhibitor Synthesis. Electrochemical studies complemented by computational analysis were implemented to investigate the anticorrosive activity of two selected unsubstituted (**1**) and bromine substituted (**2**). The synthetic methodology and comprehensive characterization of these derivatives have been reported in a prior work by El-Faham et al.,[28] as illustrated in Scheme 1. Characterization of inhibitors (**1**) and (**2**) by ^{1}H NMR, ^{13}C NMR, mass spectrometry (MS), and Fourier-transform infrared (FTIR) is reported in Supporting Information S1. Also, FTIR spectra of *s*-triazine/anilino-morpholino derivatives (**1**) and (**2**) are presented in Supporting Figure S1a,b.

Corrosion-Inhibition Studies. *Weight Loss Measurements.* Carbon steel samples were immersed in an HCl solution without or with addition of inhibitors (200 ppm) for 3 days or 7 days without the addition of an inhibitor (blank tube). The steel samples were then washed, dried, and weighed. The corrosion rate was calculated from eq 1[29]

$$C_R = \frac{\Delta W}{A \times t} \tag{1}$$

where ΔW (mg) is the weight loss of the steel sample, A is the surface area of specimens (cm^2), and t is the immersion time (h). The percent inhibition efficiency IE% was calculated from eq 2[30]

$$\text{IE\%} = \frac{(C_{R(0)} - C_{R(i)})}{C_{R(0)}} \times 100 \tag{2}$$

where $C_{R(0)}$ and $C_{R(i)}$ represent the corrosion rates in uninhibited and inhibited cases, respectively.

The following results were obtained for the 3-day experiment. The corrosion rate C_R (mg cm^{-2} h^{-1}) was 0.6126, 0.0080, and 0.0075 for the blank, (**1**), and (**2**), respectively. The inhibition efficiency IE% was 98.69 and 98.77 for (**1**) and (**2**), respectively. After the 7-day experiment, the inhibition efficiency dropped only slightly. The corrosion rate C_R (mg cm^{-2} h^{-1}) was 0.5756, 0.0128, and 0.0088 for the blank, (**1**), and (**2**), respectively. The inhibition efficiency IE% was 97.78 and 98.47 for (**1**) and (**2**), respectively. Thus, the weight loss

https://doi.org/10.1021/acsomega.4c02569
ACS Omega 2024, 9, 31714−31731

Scheme 1. Synthetic Methodology *s*-Triazine/anilino-morpholino Derivatives: Unsubstituted (1) and Bromine Substituted (2)

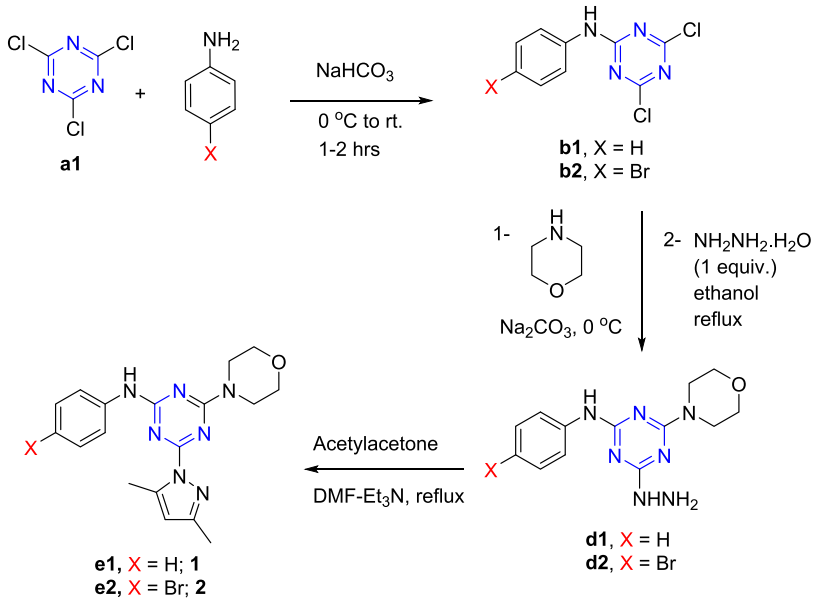

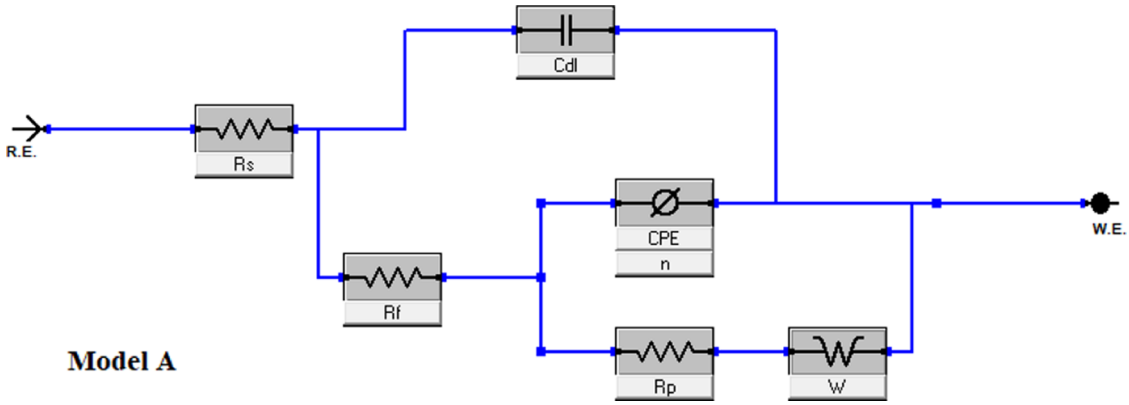

Figure 2. Equivalent circuit model A used to fit the impedance data of the *s*-triazine/anilino-morpholino derivatives.

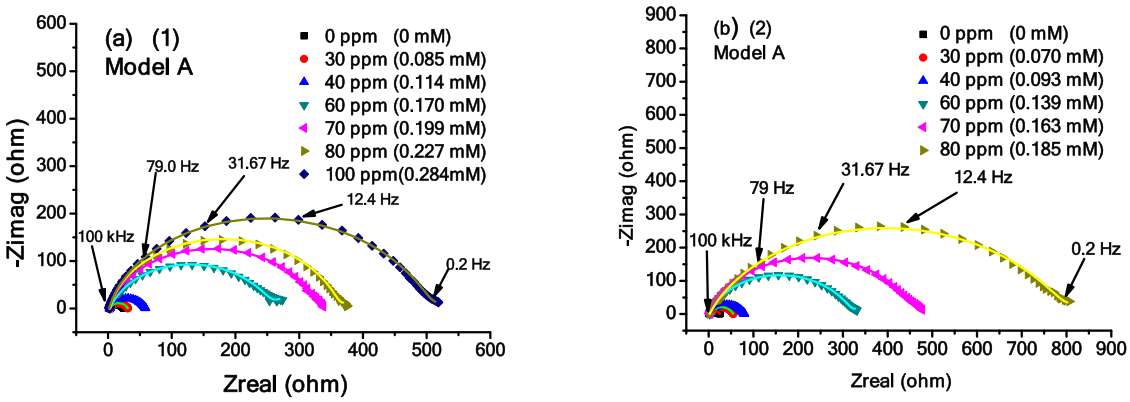

Figure 3. Nyquist plots for all concentrations of (a) inhibitor (**1**) and (b) inhibitor (**2**) in 1 M HCl at 298 K fitted by model A.

experiment at various exposure periods of 3 and 7 days ensured that the corrosion inhibition by (**1**) and (**2**) was robust, at least with respect to the exposure period studied.

Electrochemical Impedance. At the start of the experiment, the open-circuit potential E_{ocp} was conducted for 1 h in 1 M HCl to reach a steady current value on the C-steel surface. The open-circuit potential (OCP) was measured at different concentrations of inhibitors (**1**) and (**2**) in 1 M HCl for 1 h. The system reached almost a steady state after 15 min of the OCP test. But still, 1 h was chosen as the stabilization time for further electrochemical impedance study (EIS) and polarization experiments. As the concentration of (**1**) increased, at zero time, the values of OCP increased with increasing concentration. However, at the stabilization stage, the OCP

https://doi.org/10.1021/acsomega.4c02569
ACS Omega 2024, 9, 31714−31731

values decreased compared to the OCP value in the blank (Supporting Figure S2a,b) for inhibitors (**1**) and (**2**). A similar observation and trend with increasing concentrations were obtained for inhibitor (**2**).[31]

The displacement in OCP with addition of (**1**) was 31.0 mV and with (**2**) was 57.8 mV, compared to the blank. This displacement was less than 85 mV, suggesting that the compounds behaved as a mixed-type inhibitor.[32]

Electrochemical impedance studies (EISs) were then performed at a potential amplitude of 10 mV in frequencies ranging from 100,000 to 0.1 Hz. The EIS response was fitted with an equivalent electrical circuit (EEC) model A (Figure 2). The impedance results were shown as Nyquist plots (Figure 3a,b) for the inhibitors, *s*-triazine/anilino-morpholino derivatives: unsubstituted (**1**) and bromine substituted (**2**). The equivalent electrical circuit model A contains, in addition to solution resistance, two time constants. The first one has a double-layer capacitor C_{dl} and a film resistance R_f, while the second time constant has a constant-phase element CPE, a charge-transfer resistance R_{ct}, and a Warburg impedance W.[33,34] It is clear that an increase in the concentration of the inhibitor caused a wider diameter of the Nyquist plot, a higher R_{ct} value, smaller electrical current flow (I), and a higher percent inhibition efficiency IE% (Figure 3) and (Table 1). The lowest concentration is chosen such as it gives the slightest observable inhibition above the blank in the Nyquist plots. The concentration is then increased until there is no more increase in the radius of Nyquist plots and, thus, no increase in IE%. The highest inhibition performance, 97.37%, occurred for (**2**) at the optimum 80 ppm, which was higher than that of (**1**) 95.81% at the optimum 100 ppm. The inhibition did not increase above these optimum concentrations.[35] Compounds (**1**) and (**2**) are soluble in a solution made of 0.5 mL of DMSO with 12 mL of 1 M HCl at the optimum concentrations used in the electrochemical experiments. The polar para-substituents Br on the aniline group of the inhibitor (**2**) enhanced the solubility of inhibitors in aqueous acidic media. Also, bromine having lone electron pairs can act as a Lewis base that donates electrons to Fe of the electrode surface. This can explain the slight increase in inhibition efficiency of (**2**) (98.5%) compared to (**1**) (97.8%).[36,37]

The value of the CPE frequency exponent "n" decreased with increasing concentration of inhibitors (**1**) and (**2**). This can be due to the insulation of the metal/solution interface by forming a surface film. The protecting film caused an increase in the film resistance R_f and the charge-transfer resistance R_{ct}. The R_f ($\Omega\cdot cm^2$) increased from 0.357 for the blank to 5.019 and 1.612 for the inhibitors (**1**) and (**2**) at their highest optimum concentration. Similarly, R_{ct} ($\Omega\cdot cm^2$) values increased from 10.51 for the blank to 250.95 and 389.99 for inhibitors (**1**) and (**2**). Thus, the protection property of the film improved as the inhibitor concentration increased.[31] This was also supported by a decrease in CPE and C_{dl} values at the highest concentration of the inhibitors, which further indicated improvement in the reduction of the corrosion rate of C-steel. The C_{dl} ($\mu F/cm^2$) values decreased from 140 for the blank to 12.4 for (**1**) and 3.0 for (**2**) at their highest concentrations. Warburg impedance W ($Ss^{1/2}$) also decreased with an increase in the concentration from 0.68 for the blank to 0.14 and 0.06 for (**1**) and (**2**), respectively.

Log|Z| was plotted against log$f$ for (**1**) and (**2**), respectively, where Z (ohms) is the imaginary part of impedance and f (Hz)

Table 1. Impedance Parameters for Inhibitors (1) and (2) on the C-Steel in a 1 M HCl Medium by Fitting Equivalent Circuit Model A

C ppm (mM)	$R_s \pm 0.04$ ($\Omega\cdot cm^2$)	$R_f \pm 1.8$ ($\Omega\cdot cm^2$)	$R_{CT} \pm 4.17$ ($\Omega\cdot cm^2$)	$Z_{CPE} \pm 2 \times 10^{-6}$ ($\mu\Omega^{-1} s^n cm^{-2}$)	$n \pm 0.014$	$C_{dl} \pm 3 \times 10^{-6}$ ($\mu F\ cm^{-2}$)	χ^2	θ	IE% ± 0.50	$W \pm 1.2$ ($Ss^{1/2}$)
(1)										
blank (0)	1.28	0.357	10.51	975.33	0.718	140.0	0.000169	0.000	0.00	0.68
30 (0.085)	0.23	0.880	14.18	496.72	0.859	100.0	0.000232	0.259	25.89	1.10
40 (0.114)	1.15	0.653	27.28	330.61	0.769	50.1	0.000112	0.615	61.48	0.98
60 (0.170)	1.14	1.029.	125.72	190.85	0.773	12.2	0.000177	0.916	91.64	0.06
70 (0.199)	1.10	3.065	165.19	104.93	0.708	15.0	0.000057	0.936	93.64	0.66
80 (0.227)	1.12	1.177	197.82	95.58	0.790	22.3	0.000093	0.942	94.16	012
100 (0.284)	1.08	5.019	250.95	84.07	0.702	12.4	0.000089	0.958	95.81	0.14
(2)										
blank (0)	1.28	0.357	10.51	975.3	0.718	139.7	0.000169	0.000	0.00	0.68
30 (0.070)	1.19	0.633	25.44	302.4	0.781	48.8	0.000086	0.587	58.68	1.27
40 (0.093)	1.31	0.743	37.27	341.8	0.762	42.3	0.000073	0.718	71.80	0.70
60 (0.139)	1.13	1.252	158.40	161.8	0.754	15.6	0.000039	0.934	93.36	0.09
70 (0.163)	1.24	1.613	230.29	105.5	0.738	11.1	0.000043	0.954	95.44	0.07
80 (0.185)	1.06	1.612	398.99	96.5	0.704	3.0	0.000140	0.974	97.37	0.06
100 (0.233)	1.05	0.905	251.25	122.3	0.782	7.4	0.000205	0.958	95.82	0.02

https://doi.org/10.1021/acsomega.4c02569
ACS Omega 2024, 9, 31714−31731

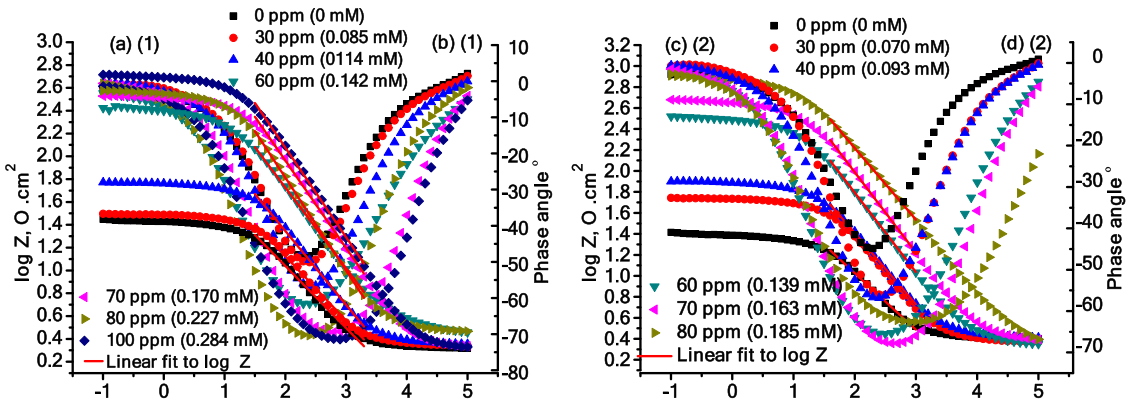

Figure 4. Bode and Bode phase plots of a C-steel electrode in a 1 M HCl solution at various concentrations of inhibitors (a, b) (**1**) and (c, d) (**2**).

Table 2. Phase Angles and α Values (Slopes) from the Bode Phase and Bode Plots for Inhibitors (1) and (2) at Various Concentrations

inhibitor	*C* ppm (mM)	0 (0)	30 (0.085)	40 (0.114)	60 (0.170)	70 (0.199)	80 (0.227)	100 (0.284)
(1)	phase angle (deg)	−48.67	−50.1	−56.69	−61.59	−69.46	−70.38	−71.42
	frequency (Hz)	198.6	252.4	252.4	252.4	627.8	252.4	796.9
	slope (α)	−0.5224	−0.5420	−0.6268	−0.7069	−0.7576	−0.8133	−0.7779
	R^2	0.9869	0.9887	0.9931	0.9990	0.9955	0.9993	0.9968
	C ppm (mM)	0 (0)	30 (0.070)	40 (0.093)	60 (0.139)	70 (0.163)	80 (0.185)	100 (0.233)
(2)	phase angle (deg)	−48.67	−56.08	−56.79	−65.54	−67.78	−62.43	−67.12
	frequency (Hz)	198.6	315.5	252.4	315.5	398	627.8	315.5
	slope (α)	−0.5401	−0.6637	−0.6802	−0.7583	−0.7667	−0.6838	−0.7247
	R^2	0.9947	0.9952	0.9983	0.9995	0.9990	0.9992	0.9968

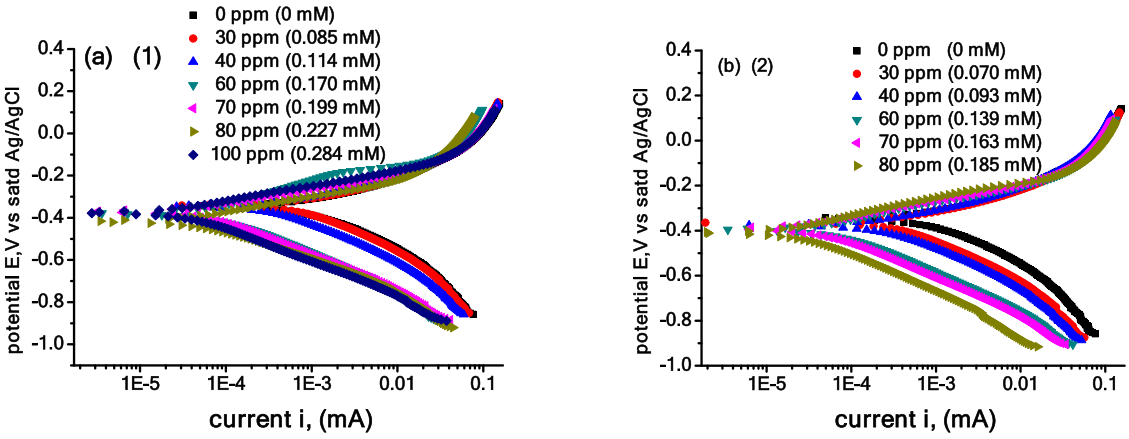

Figure 5. Tafel plots for all concentrations of (a) inhibitor (**1**) and (b) inhibitor (**2**) in 1 M HCl at 298 K.

is the frequency (Bode plots) (Figure 4a,b). The slope of linear region α increased from the blank value −0.530 to −0.778 for 100 morpho-H and to −0.684 for 100 ppm morpho-Br, respectively. This revealed that the inhibitor caused the surface of the C-steel to become less coarse,[30] while the log *Z* value at $\log f = -1$ increased from 1.42 for the blank to 2.72 for morpho-H and 2.90 for morpho-Br, both at 100 ppm. This also supported strong inhibition performance by morpho-H and morpho-Br for C-steel corrosion in a hydrochloric acid solution (Table 2).[38]

Additionally, increasing the inhibitor concentration resulted in shifting the peak phase angle toward more negative values; see Bode phase angle plots (Figure 4a,b) for (**1**) and (**2**), respectively. The phase angle values increased from −48.67° for the HCl blank solution to −71.42° for 100 ppm of (**1**) solution and to −62.43° for 80 ppm of (**2**) solution (Table 2).[38] As the concentration of the added inhibitors to the acid solution increased, the peaks in the Bode phase plots became wider and shifted to a higher frequency. This is because the inhibitor molecules were adsorbed onto the steel surface, and a protective layer was formed.[39]

Potentiodynamic Polarization. Potentiodynamic polarization PDP was measured from −900 to 200 mV vs saturated Ag/AgCl with a scan rate of 5 mV/s. Figure 5 shows the polarization curves for C-steel in 1 M HCl at various inhibitor concentrations. The % IE values of the compounds, obtained by PDP technique (Table 3), matched those obtained by the EIS technique. They were 98.5% for (**2**) and 97.8% for (**1**) at a concentration of 80 and 100 ppm, respectively.

https://doi.org/10.1021/acsomega.4c02569
ACS Omega 2024, 9, 31714−31731

Table 3. Polarization Parameters for Various Concentrations of Inhibitors (1) and (2) on C-Steel in 1 M HCl

inhibitor	C ppm (mM)	β_a (V dec^{-1})	$-\beta_c$ (V dec^{-1})	i_{corr} (mA)	E_{corr} (mV) ± 20	CR (mpy)	χ^2	i_{corr} (mA/cm^2)	θ	IE% ± 0.50
(1)	0 (0)	0.2468	0.3293	2.237	−345.9	2034	13.40	4.450	0.000	0.0
	30 (0.085)	0.2273	0.3085	1.765	−340.9	1604	18.34	3.511	0.211	21.1
	40 (0.114)	0.1924	0.2596	0.757	−346.1	688	28.16	1.505	0.662	66.2
	60 (0.170)	0.1498	0.1929	0.091	−378.8	82.5	27.06	0.181	0.959	95.9
	70 (0.199)	0.1384	0.1861	0.078	−370.9	71.62	42.18	0.157	0.965	96.5
	80 (0.227)	0.1534	0.1756	0.083	−417.6	75.11	43.67	0.164	0.963	96.3
	100 (0.284)	0.1307	0.1764	0.048	−376.3	44.08	39.00	0.097	0.978	97.8
(2)	0 (0)	0.2468	0.3293	2.237	−345.9	2034	13.4	4.450	0.000	0.0
	30 (0.070)	0.1956	0.2685	0.823	−364.9	748.2	26.98	1.637	0.632	63.2
	40 (0.093)	0.1863	0.2413	0.491	−376.1	445.8	28.02	0.976	0.781	78.1
	60 (0.139)	0.1416	0.1856	0.088	−394.1	80.09	35.55	0.175	0.961	96.1
	70 (0.163)	0.1355	0.1825	0.059	−391.1	54.03	37.75	0.118	0.973	97.3
	80 (0.185)	0.1273	0.1862	0.034	−408.6	30.91	35.22	0.068	0.985	98.5
	100 (0.233)	0.1304	0.1645	0.033	−454.5	30.56	35.09	0.067	0.985	98.5

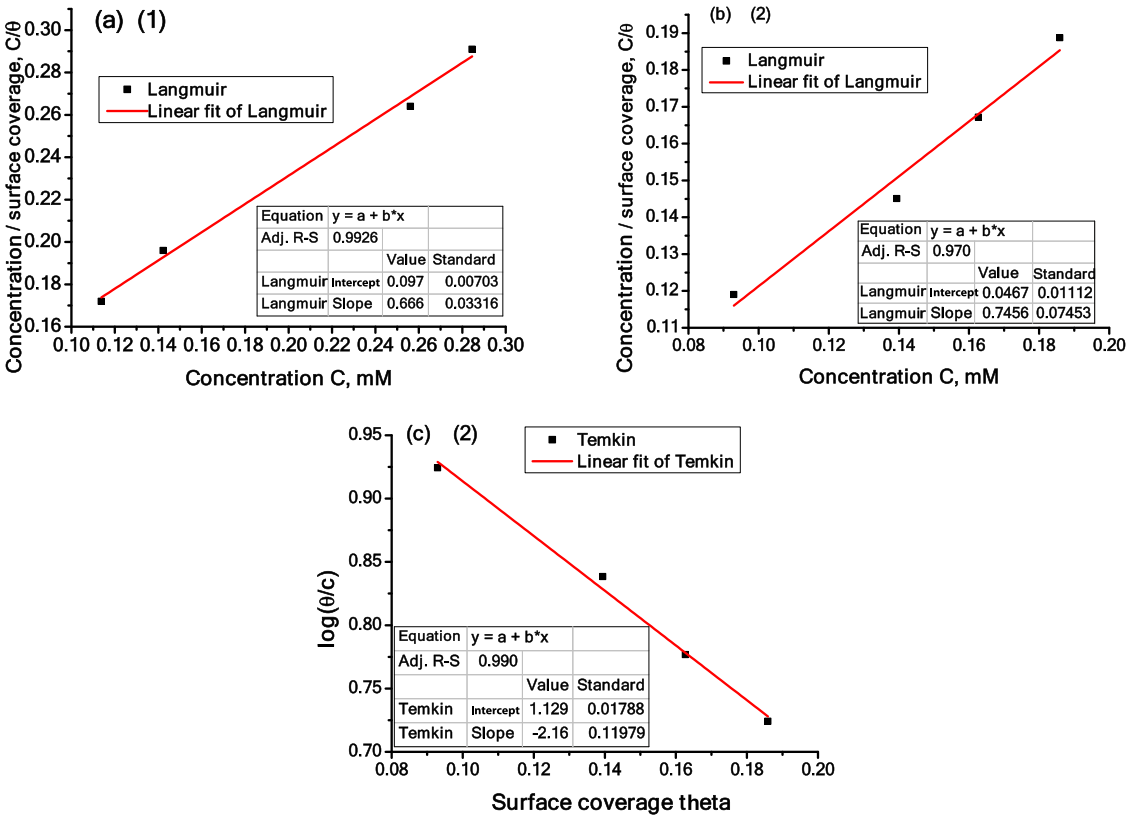

Figure 6. Adsorption isotherm from Tafel plots (a) for the (**1**) Langmuir model, the (**2**) (b) Langmuir model, and the (c) Temkin model on C-steel in a 1 M HCl solution.

Both the anodic Tafel slopes (β_a) and the cathodic Tafel slopes (β_c) decreased with an increase in the concentration of inhibitors. As the concentration of inhibitors increased (Table 3), the values of cathodic slope β_c (mV dec^{-1}) decreased from −0.3293 for the blank to −0.1764 for the inhibitor (**1**) and to −0.1862 for the inhibitor (**2**), while the anodic slope β_a (mV dec^{-1}) decreased from 0.2468 (blank) to 0.1307 (inhibitor (**1**)) and to 0.1273 (inhibitor (**2**)). This indicated that better inhibition efficiency occurred at higher concentrations of inhibitors.[30] It was also found that the corrosion potential increased slightly with the addition of inhibitors, while the corrosion current density I_{corr} and the corrosion rate CR decreased from 4.450 mA/cm^2 and 2034 mpy for the blank solution to 0.068 and 30.91 for (**2**) and to 0.097 and 44.08 for (**1**), respectively, at their optimum concentrations (Table 3). Thus, (**2**) with smaller values of I_{corr} and CR than those of (**1**) is a better inhibitor of corrosion toward C-steel in 1 M HCl. This is related to the effect of the electron-donor Br substituent.

The variation of the cathodic branch toward more negative potential with increasing concentration of inhibitors compared to a 1 M HCl blank solution was more obvious than in the case of the shift of the anodic branch toward positive potential values. This revealed that the corrosion inhibition was dominated by the cathodic process.[40] Therefore, the inhibitors (**1**) and (**2**) exerted dominant cathodic inhibition toward corrosion of C-steel. Thus, the s-triazine/anilino-morpholino derivatives promoted inhibition of corrosion by a decrease in

https://doi.org/10.1021/acsomega.4c02569
ACS Omega 2024, 9, 31714−31731

Table 4. Comparison of the Inhibitor Structure, IE%, Maximum Dose, Adsorption Isotherm, and Nature of Inhibition for Steel in 1 M HCl

Inhibitor structures	Metal/Medium	Optimum Concentration IE%	Adsorption isotherm [Nature of inhibition]	Reference
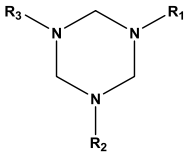 R1 = R2 = R3 = 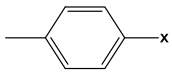 X = H X = CH_3 X = OCH_3 X = NH_2 X = NO_2	Mild steel/ 1M HCl	(300 ppm) 92.66% 93.67% 94.95% 97.07% 84.80%	Langmuir (Mixed)	[45]
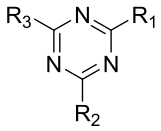 R_1=R_2=R_3 = 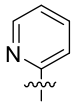	Mild steel/1M HCl	(312 ppm) 89.3%	Langmuir (Mixed)	[18]
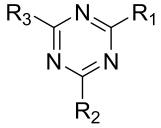 R_1=R_2=R_3 = 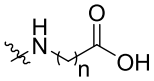 n = 1 n = 2 n = 3	Mild Steel/1M HCl	(5000 ppm) 71.8% 76.5% 81.7%	Langmuir (Mixed)	[46]
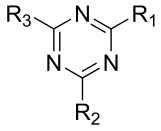 R_1 =R_3 = NH_2NH- R_2 = 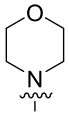	Steel /1M HCL	(225 ppm) 98%	Langmuir (Mixed)	[23]
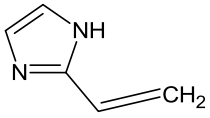	Mild steel/ 1 M HCl	10 mM (82.3 %)	Langmuir (Mixed)	[47]

https://doi.org/10.1021/acsomega.4c02569
ACS Omega 2024, 9, 31714−31731

Table 4. continued

Inhibitor structures	Metal/Medium	Optimum Concentration IE%	Adsorption isotherm [Nature of inhibition]	Reference
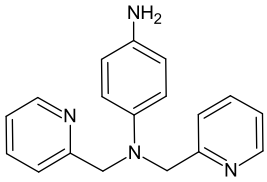	Mild Steel/ 1 M HCl	2 mM (81%)	Langmuir (Mixed)	[48]
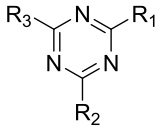 R1 = 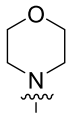 R2 = 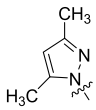	C-steel/ 1M HCl			Present work
R_3 = 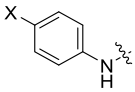				
X = H		(100ppm) 97.8%	Langmuir (Cathodic)	
X = Br		(80ppm) 98.5%	Temkin (Cathodic)	

hydrogen evolution and dissolved oxygen reduction in an aerated hydrochloric acid solution.

Adsorption isotherms were studied to gain information about the interactions between the inhibitors and the C-steel electrode surface. Three isotherm models were tested: Langmuir, Temkin, and Frumkin. The values of fractional surface coverage (θ) calculated from potentiodynamic polarization were used to fit the isotherm models. Based on the highest correlation coefficient, R^2, the Temkin adsorption model explained better the adsorption behavior of the inhibitor (**2**) with R^2 = 0.990 (Figure 6c), while Langmuir (Figure 6b) and Frumkin models gave R^2 values of 0.970 and 0.936, respectively. The best adsorption isotherm for (**1**) was the Langmuir model (R^2 = 0.992) (Figure 6a) compared to Temkin (R^2 = 0.946) and Frumkin (R^2 = 0.940).[41] The equilibrium adsorption constant K_{ads} computed from the inverse of the intercept of the Langmuir plot was equal to 1.074×10^4 L/mol for (**1**) and 2.141×10^4 L/mol for (**2**). Accordingly, the free energy change of adsorption ΔG_{ads} computed from K_{ads} was −32.97 (kJ/mol) for (**1**) and −34.68 (kJ/mol) for (**2**). Thus, the adsorption of morpholine derivatives onto C-steel involved physical and chemical adsorption (comprehensive adsorption).[42]

Inhibition Mechanism. In weak acidic media, the triazines exist as neutral or protonated species.[43] The exposure of the C-steel surface to HCl (1 M) resulted in the oxidation of Fe to Fe^{2+}, which attracted Cl^-, rendering the surface of steel negatively charged.[44] Also, HCl can cause protonation of various N atoms of the inhibitor to form protonated inhibitor species. Physical adsorption can be due to the electrostatic attraction between the negatively charged surface of steel and the positively charged protonated inhibitor, while chemical adsorption can occur due to the complexation of Fe^{2+} with the neutral inhibitor molecules, which have electron-rich groups that can donate electrons from their π bonds such as >C═N of imine of triazine and diazole rings, >C═C< of the phenyl ring group, or from their free electrons pair of nitrogen and oxygen atoms. Additionally, inhibitor (**2**) contains a bromine atom that can σ bond to Fe^{2+} and enhance adsorption compared to inhibitor (**1**), which lacks a halogen atom. This can explain the increase in the inhibition efficiency of (**2**) compared to (**1**). Physical and chemical adsorption of the inhibitor caused the formation of a protective film on the surface of steel and hindered the attack of H^+ necessary to produce hydrogen gas on the cathodic site and thus improved inhibition. Also, the planarity and larger molecular size of studied molecules ensured formation of a larger protective film on mild steel and improves inhibition of corrosion.[45]

Comparative Inhibition Studies of Different Inhibitors. The inhibitors (**1**) and (**2**) containing triazine, with branches anilino, diazole, and morpholino moieties in one molecule (Table 4), showed better inhibition efficiency than the hexahydrotriazine derivatives,[45] better than other reported *s*-triazine derivatives with three pyridyl groups,[18] with three amino carboxylic acid branches,[46] two hydrazinyl groups and one morpholine group (higher inhibitor concentration used),[23] and much better than both vinyl imidazole[47] and 4-amino-*N*,*N*-di(2-pyridylmethyl)-aniline.[48] Thus, the presence of heteroatoms and aromatic rings in the inhibitor molecule affects the overall inhibition efficiency.

Surface Analysis. The scanning electron microscopy SEM technique was adopted to study the microscopic surface morphology of C-steel immersed in a blank solution (HCl 1 M) for 4 h (Figure 7). The morphology for the steel immersed

https://doi.org/10.1021/acsomega.4c02569
ACS Omega 2024, 9, 31714−31731

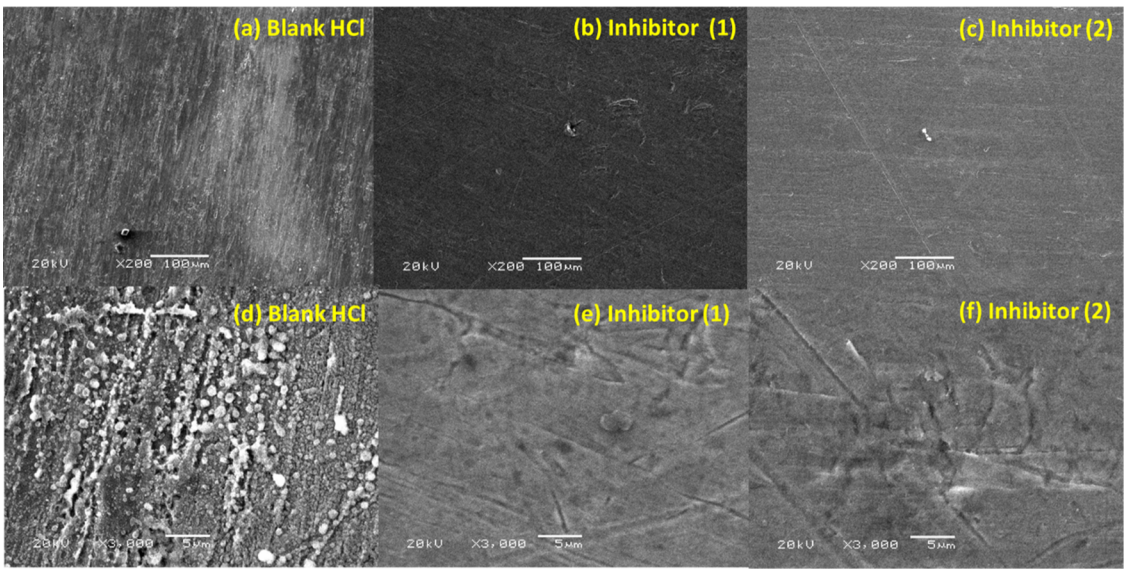

Figure 7. SEM micrographs for C-steel immersed in 1 M HCl for 4 h (a, d), with added (**1**) 100 ppm (b, e), and with added (**2**) 100 ppm (c, f) with magnifications of (×200) and (×3000), respectively.

in blank HCl (1 M) indicated that the surface was very corroded and very porous Figure 7(a,d). Also, at higher magnification, white spherical particles were observed due to the corrosion products from the iron surface, which can be iron oxide wustite FeO, hematite Fe_2O_3 and magnetite Fe_3O_4, and also iron oxy-hydroxide FeOOH nanoparticles (Figure 7d).[49,50] While in the case of steel immersed in HCl (1 M) in the presence of inhibitors (**1**) and (**2**), Figure 7(b,e,c,f) shows that the surface of steel was protected, as it looked smooth. Also, there was the absence of white iron oxide corrosion products.

Quantum Chemical Study of the Inhibitor Global Reactivity. The electronic structure of *s*-triazine/anilino-morpholino derivatives, unsubstituted (**1**) and bromine substituted (**2**) in gaseous and aqueous phases considered in this work, was determined using the B3LYP method with 6-311+G(d,p) (Table S1). The nitrogen heteroatoms found within the inhibitors are prone to protonation in a 1 M aqueous hydrochloric acid medium. Consequently, the computational calculations of the protonated species in both gaseous and aqueous phases are also conducted to ensure stability (Table S2). The calculated parameters of the neutral morpholine derivatives displayed minor variation between the inhibitor in the gaseous and aqueous phases. Thus, the results of studied inhibitors in the aqueous phase are tabulated in Table 5, whereas the calculated values of the gaseous phase are included in Table S3.

Since, under the experimental conditions, the prototyped inhibitors exhibit nitrogen heteroatoms that are prone to protonation and which are in the aqueous phase, we summarized the calculated parameters of the protonated species in the aqueous phase in Table 5. However, the results of the gaseous phase can be found in Table S4.

The FMOs (HOMO and LUMO) are very formidable in predicting the chemical reactivity of the studied inhibitors. The electrons in the highest occupied molecular orbital (HOMO) are linked to the molecule's ability to donate electron, whereas the lowest unoccupied molecular orbital (LUMO) is associated with its ability to obtain electron. The electron-donor capacity of inhibitors increases with increasing energy of the HOMO (E_{HOMO}), which demonstrates better inhibitory activity on a metal surface. Alternately, the electron-acceptor characteristic increases with decreasing energy of the LUMO (E_{LUMO}). Furthermore, the energy difference between these orbitals (HOMO and LUMO), ΔE, determines the kinetic stability, chemical reactivity, optical polarizability, and chemical hardness−softness of a compound.[51] Smaller values of ΔE reflect lower electronic stability, and hence higher reactivity. It implies that the electronic excitation from the HOMO to LUMO promotes better efficiency.

Table 5. Some Chemical Parameters for the Neutral and Protonated Forms of (1) and (2) in the Aqueous Phase Calculated with the B3LYP Method with the 6-311+ +G(d,p) Basis Set

	neutral form		protonated form	
parameters	(**1**)	(**2**)	(**1**)	(**2**)
E_{HOMO}, eV	−6.22	−6.231	−6.932	−6.687
E_{LUMO}, eV	−1.422	−1.484	−2.300	−2.391
ΔE, eV	4.798	4.747	4.631	4.296
DM, D	3.536	3.334	8.871	12.864
I, eV	6.22	6.23	6.93	6.69
A, eV	1.42	1.48	2.30	2.39
χ, eV	3.82	3.86	4.62	4.54
η, eV	2.40	2.37	2.32	2.15
S, eV^{-1}	0.42	0.42	0.43	0.47
μ, Ev	−3.82	−3.86	−4.62	−4.54
ω, eV	17.51	17.66	7.20	7.33
$\Delta E_{B\text{-}d}$, eV	−0.60	−0.59	−0.58	−0.54
ΔN	0.66	0.66	0.51	0.57
IE, %	97.8	98.5	97.8	98.5

The computed E_{HOMO}, E_{LUMO}, and ΔE values of the neutral (**1**) and (**2**) in the aqueous phase tabulated in Table 5 depicted that (**2**) exhibited greater E_{HOMO} and lower E_{LUMO} with a smaller ΔE value. This agrees very well with the experimental data and implies that (**2**) is a more effective corrosion inhibitor than (**1**). Figure 8b displays the FMO diagrams of the neutral species.

https://doi.org/10.1021/acsomega.4c02569
ACS Omega 2024, 9, 31714−31731

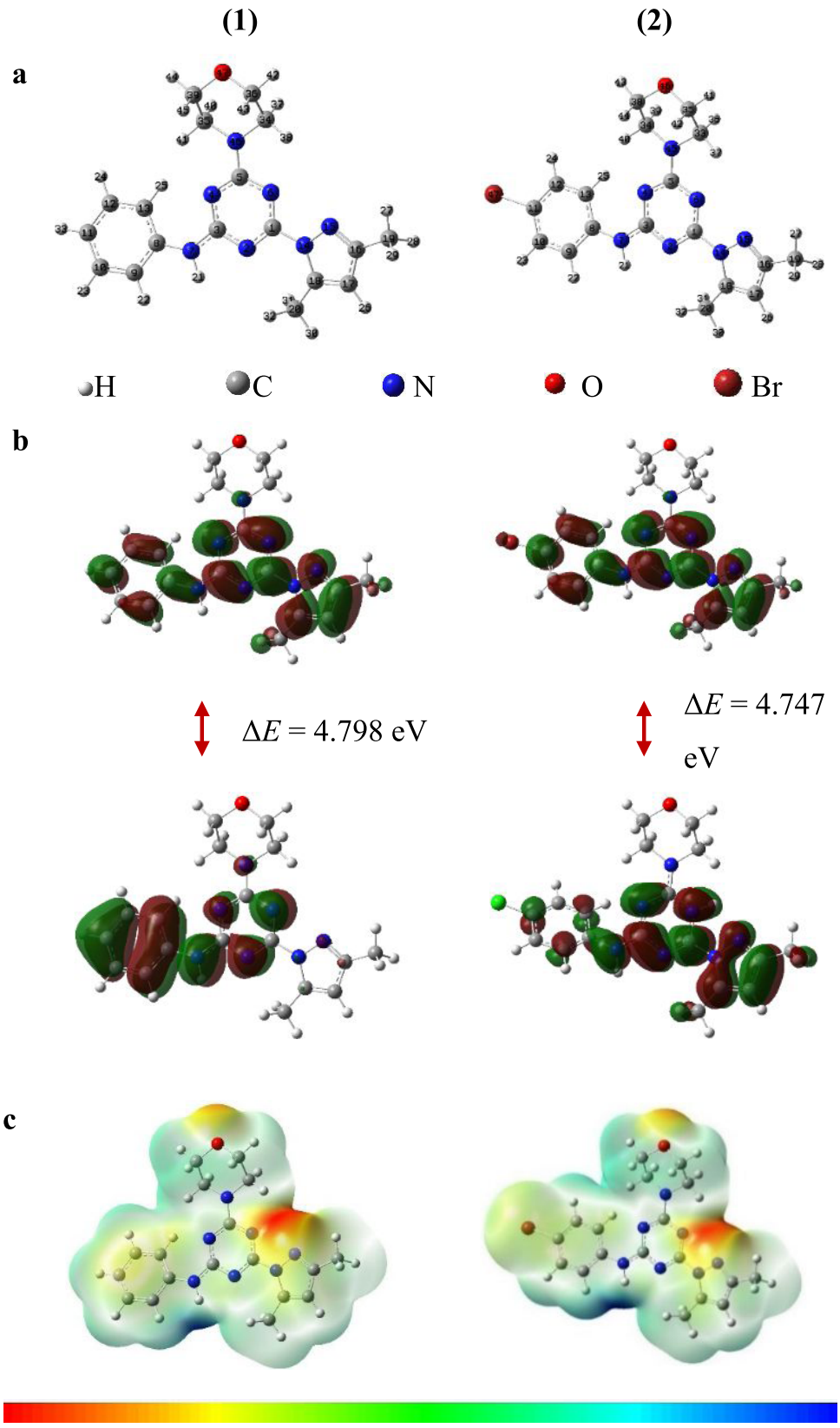

Figure 8. Quantum chemical calculations by the B3LYP method with the 6-311++G(d,p) basis set: (a) Optimized molecular structure, (b) frontier molecular orbitals, and (c) electrostatic potential mapping of neutral (**1**) and (**2**) in the aqueous phase. In (b), green indicates a positive orbital wave function, while red represents a negative orbital wave function. In (c), red indicates a high electrostatic potential, while blue indicates a low electrostatic potential.

The theoretical calculations of the protonated morpholine derivatives found in Table 5 also unveil similar trends, where (**2**) displayed higher E_{HOMO}, lower E_{LUMO}, and smaller ΔE values than (**1**). The optimized structure of the FMO diagrams

https://doi.org/10.1021/acsomega.4c02569
ACS Omega 2024, 9, 31714−31731

of the protonated species in aqueous media are shown in Figure 9a.

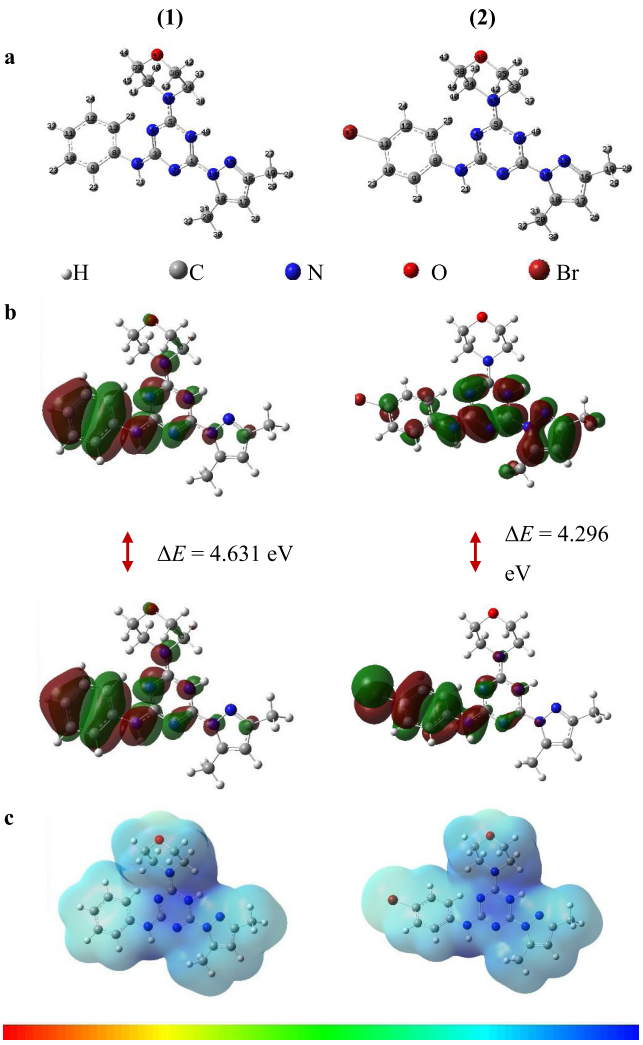

Figure 9. Quantum chemical calculations by the B3LYP method with the 6-311++G(d,p) basis set: (a) Optimized molecular structure, (b) frontier molecular orbitals, and (c) electrostatic potential mapping of protonated (**1**) and (**2**) in the aqueous phase. In (b), green indicates a positive orbital wave function, while red represents a negative orbital wave function. In (c), red indicates a high electrostatic potential, while blue indicates a low electrostatic potential.

Another essential descriptor that also interprets a molecule's chemical reactivity is known as the ionization potential (I). The smaller I value means lower molecular stability as well as their chemical inertness and, thus, higher reactivity. Meanwhile, a higher I reflects the opposing effect.[52] The protonated (**2**) inhibitor has a lower I at 6.69 eV in an aqueous phase, in contrast to (**1**) at I = 6.93 eV, which indicates higher inhibition efficiency (IE) of (**2**). In the neutral form, we are unable to come up with a valid comparison as the I values are in close proximity to one another. The dipole moment (DM) of a molecule is another important electronic parameter that provides information on the polarity and the reactivity indicator. The calculated results show that (**2**) predominantly has the highest value of the dipole moment at 12.864 D in the protonated form in an aqueous phase but possesses the lowest result at 3.334 D in the neutral and aqueous phases. In the literature, the scientific community discovered both positive and negative relationships between the dipole moment and the inhibition efficiency.[53−55] Therefore, these findings restrict us from drawing a valid prediction on the inhibition efficiency based on the estimated dipole moment. A small electronegativity value (χ) of the inhibitory molecules suggests a greater tendency to donate electrons during the metal−surface interaction. Due to the very close proximity of the values, we are unable to compare them. Miniscule variations were observed between the calculated results. It demonstrated a lower inhibitory efficiency with respect to the higher χ value of the (**2**) in the neutral phase but a reverse effect in their protonated phase. Hence, the close proximity and the inconsistency restrict us from presenting a valid comparison.

Global reactivity parameters, namely, the global hardness (η) and global softness (S) reflect the chemical reactivities and chemical inertness of the studied inhibitors. Softer molecules easily offer electrons to an acceptor, and for that reason, they are more reactive than harder molecules. In corrosion science, the metal surface serves as a Lewis acid, while the studied inhibitor serves as a Lewis base. Base inhibitors are preferentially more feasible in the acidic corrosion of bulk metals (soft acid).[56] From Table 5, both η and S values of the inhibitors are again in very close proximity. The minute discrepancy between the values seems to suggest that (**2**) is the softest molecule, as shown by the slightly lower η.

The values of ΔN and $\Delta E_{\text{B-d}}$ were also calculated, as shown in Table 5. The ΔN values depict the trend of electron-donating capacities of the analyzed inhibitors. As reported by Lukovits,[57] the inhibition efficiency increased with increasing electron-donor characteristics, given $\Delta N < 3.6$. This signifies a greater propensity of the inhibitors to be adsorbed on the metal surface through donor−acceptor interactions. In this investigation, the existence of heteroatoms resulted in the interaction between the nonbonding electron pairs and the π-electrons within the inhibitors with the vacant d-orbitals on the metal surface. The calculated values of ΔN shown in Table 5 are all below 3.6, but we are unable to compare these values because they are more or less the same. The back-donation energy $\Delta E_{\text{B-d}}$ illustrates the morpholine inhibitors' interaction with the carbon steel electrode surface. As all of the values are $\Delta E_{\text{B-d}} < 0$ with $\eta > 0$, the back-donation is generally energetically preferred due to the increase in stabilization energy gained from the interactions. However, we are again unable to compare these values as the they are very close to each other. The magnitude of a molecular inhibitor in acquiring electrons can be derived from the electrophilicity index.[58] The electrophilicity (ω) values suggest (**2**) in the neutral and aqueous state (Table 5) having slightly higher electron-accepting ability at ω = 17.66 eV, whereas an opposing observation was seen in their protonated form in aqueous media. (**1**) was recorded at ω = 22.90 eV, which is higher than (2) at ω = 22.13 eV (Table 5). Hence, a valid comparison cannot be established.

Local Reactivity. Mulliken population analysis (MPA), Fukui indices, and electrostatic potential surface (ESP) are calculated to locate the active centers within the investigated morpholine derivative inhibitors. The occupancy of various active sites on the inhibitor molecule served as an advantage because they provided a greater tendency to contribute their electronic characteristics to the unoccupied d-orbitals of the C-steel metal surface.[59] Fukui indices are implemented to identify the reactivity regions and analyze the inhibitor's electrophilic

https://doi.org/10.1021/acsomega.4c02569
ACS Omega 2024, 9, 31714−31731

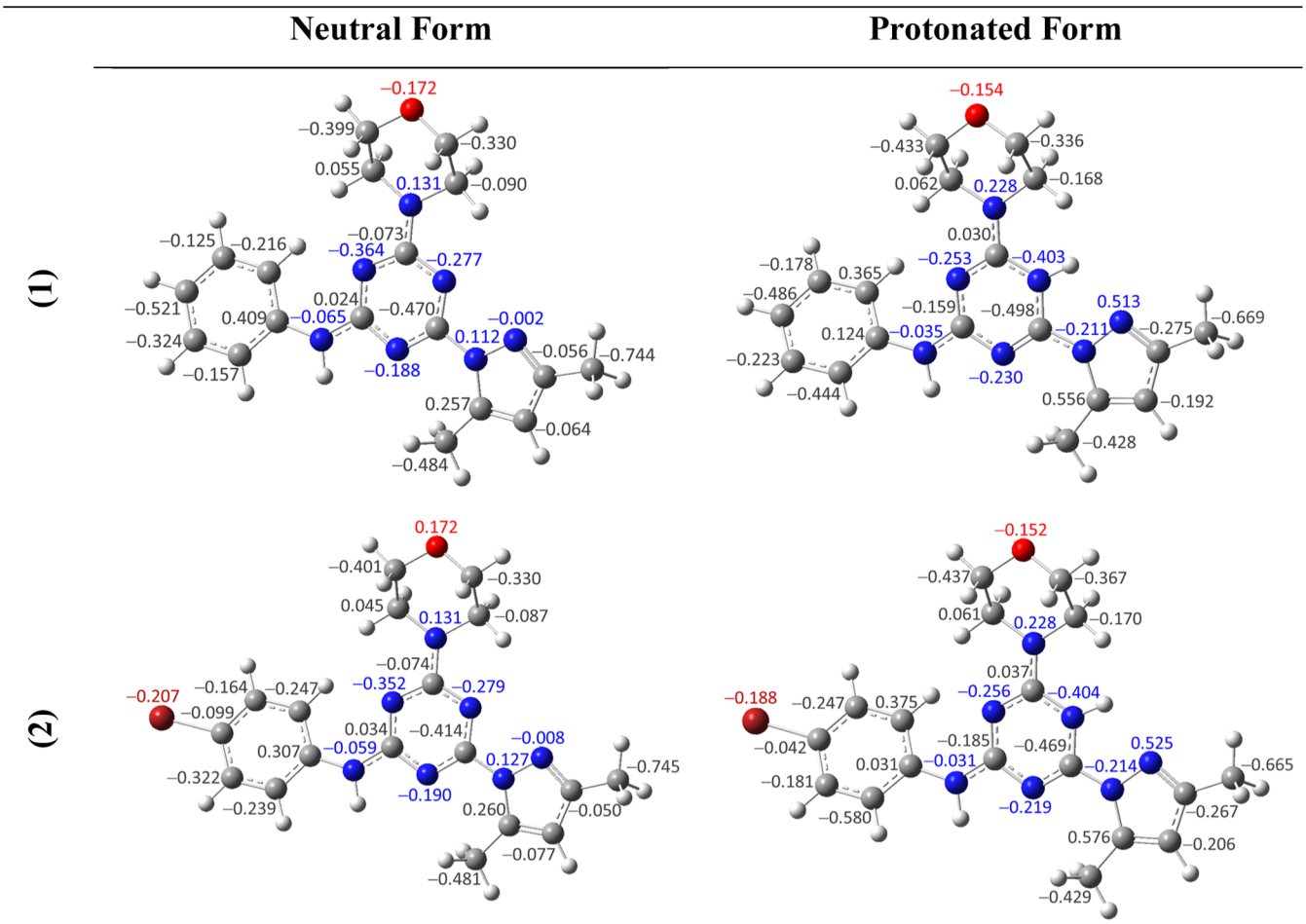

Figure 10. Mulliken charge population analysis of the neutral and protonated forms of (**1**) and (**2**) in the aqueous phase.

and nucleophilic behavior, which allows the evaluation of the local selectivity with the corrosion inhibitor.[60] Subjection of an electron to the LUMO of the neutral molecule yields an anionic species ($N + 1$), while the loss of an electron results in a cationic species ($N - 1$). A region in the molecule is considered prone to a nucleophilic attack when f_k^+ has the greatest value and $\Delta f_k > 0$. Meanwhile, when the region displayed greatest f_k^- value with $\Delta f_k < 0$, the region preferentially favored for an electrophilic attack.[61]

Speculation of the adsorption centers of the inhibitor can be attained with high precision *via* the application of the Mulliken population analysis (Table S5) and (Table S6).[53] Hence, the Mulliken charge densities of the optimized morpholine derivatives in the aqueous phase are shown in Figure 10. It was reported that the magnitude of the adsorption on the metal surface increases in the presence of more negatively charged heteroatoms because of the donor−acceptor interaction with the C-steel surface.[62] The highest negatively charged center is found on C (9) of (**1**) at −0.782 and on C (19) of (**2**) at −0.745. In the event of the protonated species, the most negatively charged adsorption site is located on C (19) at −0.669 and −0.665 of inhibitors (**1**) and (**2**), respectively.

The Fukui functions of the neutral and protonated species in the aqueous state are then calculated based on the Mulliken population analysis (MPA). The calculated Fukui functions of these species are summarized in Table S7. The favored sites for a nucleophilic attack on the neutral and aqueous morpholine derivatives are (shown by the highest values of f_k^+ and $\Delta f_k > 0$) at C1, N (4), C (11), C (13), N (15), C (17), C (18), C (35), C (36), C (39), and N (46) in inhibitor (**1**) and at C (1), N (4), N (6), C (8), C (13), N (15), C (17), C (18), C (35), and C (38) in inhibitor (**2**). The favored sites for an electrophilic attack are (shown by the highest f_k^- and more negative Δf_k) at N (2), C (3), N (6), N (7), C (8), and C (9) in inhibitor (**1**) and at N (2), C (3), N (7), C (9), C (11), C (12), C (19), C (20), C (34), N (45), and Br (47) in inhibitor (**2**). On the other hand, the favored sites for a nucleophilic attack on the protonated species in the aqueous phase are (shown by the highest values of f_k^+ and $\Delta f_k > 0$) at C (1), N (4), C (5), C (9), C (10), C (12), N (15), C (17), C (18), C (20), and N (46) in inhibitor (**1**) and C (1), N (4), C (10), C (13), N (15), C (17), C (34), and N (45) in inhibitor (**2**). The favored sites for an electrophilic attack are (shown by the highest f_k^- and more negative Δf_k) at N (2), C (3), N (6), N (7), C (11), and C (13) in inhibitor (**1**) and at N (2), C (3), N (6), N (7), C (8), C (9), C (11), C (12), C (18), C (35), C (38), and Br (47) in inhibitor (**2**).

According to Fukui indices of the neutral and aqueous phase in Table S7, C (13) at 0.813 is the most reactive site for a nucleophilic attack for species (**1**) and N (15) at 0.236 for molecule (**2**). On the other hand, C (9) at 0.652 on morpho-H is the most reactive site for an electrophilic attack, and C (12) at 0.218 on compound (**2**) is more prone to the electrophilic

https://doi.org/10.1021/acsomega.4c02569
ACS Omega 2024, 9, 31714−31731

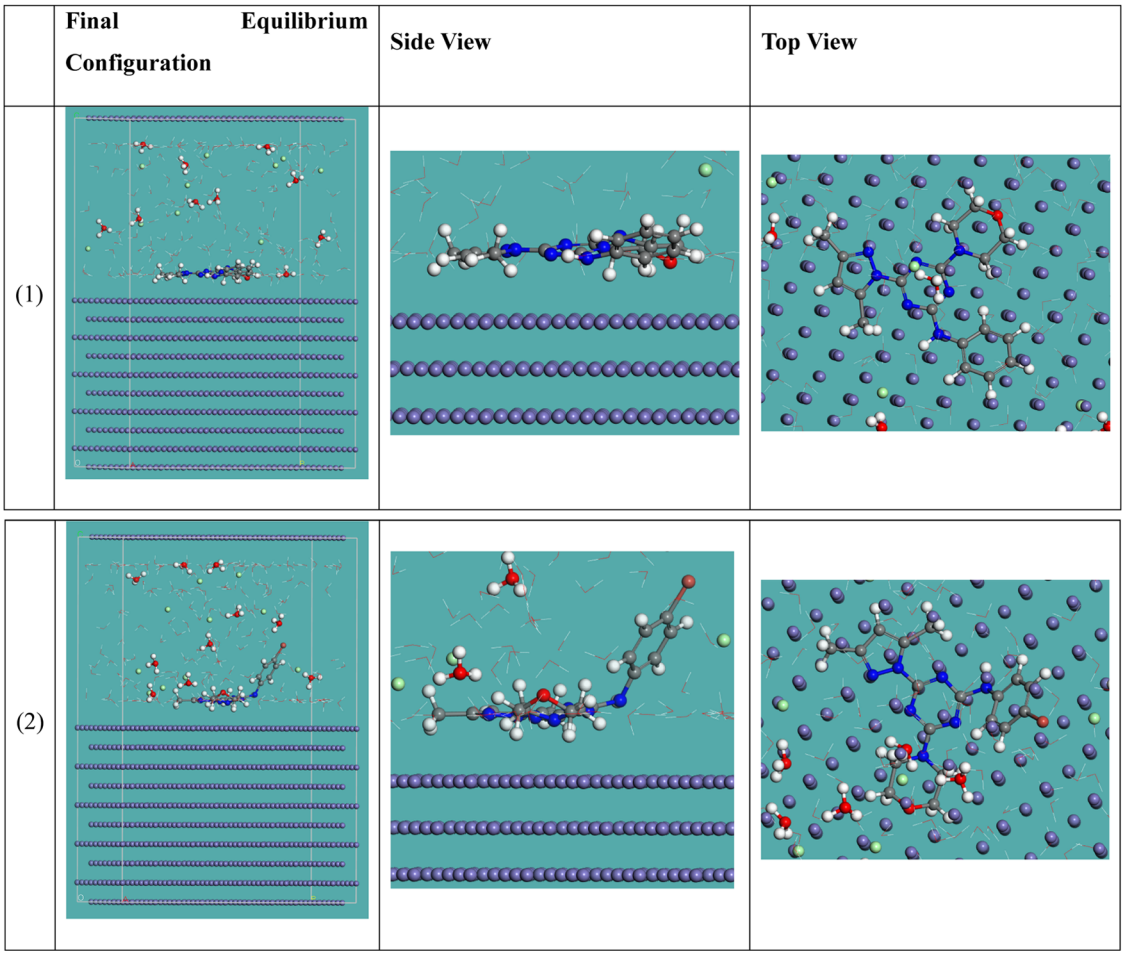

Figure 11. Highest proper adsorption arrangement for inhibitors (**1**) and (**2**) on the Fe(110) substrate obtained by the adsorption locator module.

Table 6. Data and Descriptors Calculated by the MC Simulations for the Adsorption of Inhibitors (1) and (2) on Fe(110)[a]

structures	adsorption energy	rigid adsorption energy	deformation energy	inhibitor dE_{ad}/dN_i	chloride dE_{ad}/dN_i	hydronium dE_{ad}/dN_i	water dE_{ad}/dN_i
Fe(110), molecule (1), water, hydronium, Cl^- ions	−8061.41	−4479.98	−3581.44	−371.64	−143.75	−62.86	−18.53
Fe(110), molecule (2), water, hydronium, Cl^- ions	−8084.57	−4507.80	−3576.77	−380.91	−141.40	−60.30	−18.37

[a]Energy in kcal mol^{-1}.

attack. The calculated Fukui indices of the protonated and aqueous phases suggest that N (15) at 0.273 in compound (1) is more prone to a nucleophilic attack and C (13) at 0.585 in compound (2). The adsorption sites C (13) at 0.446 and C (9) at 0.373 on the protonated inhibitors (**1**) and (**2**), respectively, are the most reactive sites for an electrophilic attack. The electron density surface mapped with the electrostatic potential surface (MEP) has been used to assess the relative reactivity of inhibitors to electrophilic and nucleophilic reactions.[63] Figures 8c and 9c represent the electrostatic potential (ESP) of the morpholine derivatives. The electron-rich and electron-poor areas of the molecular electrostatic potential (MEP) are distinguished by red and yellow (negative) and blue (positive) areas, respectively, while the neutral regions are represented by green areas. The electronic densities increased in the order red > orange > yellow > green. Figure 8c of the neutral species shows the regions of negative potential (red) that are related to the nucleophilic reactivity around the nitrogen and oxygen heteroatoms. The greatest negative potential based on the figure is around the N (6) site, which yields a greater tendency to undergo protonation in an acidic medium. The ESP of the protonated morpholine inhibitors is displayed in Figure 9c. It illustrates the electrophilic nature of the protonated species in the aqueous phase, as shown by the blue areas of the ESP structure. This somehow suggests that the inhibitor mainly possesses an electrophilic characteristic especially on the nitrogen heteroatoms.

Monte Carlo Simulations. The objective of the MC simulations was to determine the interactions between inhibitor molecules and the steel surface and gain insights into the mechanism of the adsorption process. The highest favorable adsorption arrangements for (**1**) and (**2**) molecules on the steel surface in a corrosive medium were identified using the adsorption locator module. Figure 11 shows the nearly flat orientation of the identified adsorption configurations, indicating an improvement in adsorption and maximum surface coverage.[64] Table 6 records the adsorption

https://doi.org/10.1021/acsomega.4c02569
ACS Omega 2024, 9, 31714−31731

energies obtained from the MC simulations. The data showed that (**2**) with −8084.57 kcal mol^{-1} had a more negative adsorption energy value compared to the (**1**) molecule with −8061.41 kcal mol^{-1}, indicating strong adsorption of molecule (**2**) on the steel surface. This formed a stable adsorbed film that protected the steel from corrosion, which is consistent with practical results.[65] Table 6 indicates that the rigid adsorption energy values for molecule (**2**) with −4507.80 kcal mol^{-1} were more negative than that of molecule (**1**) with −4479.98 kcal mol^{-1}, suggesting that molecule (**2**) had better protection efficiency than molecule (**1**).

The dE_{ads}/dN_i values represent the energy associated with the metal/adsorbate arrangement, excluding adsorbed H_2O molecules.[66] The dE_{ads}/dN_i values for molecule (**2**) (−380.91 kcal mol^{-1}) are higher than that of molecule (**1**) (−371.64 kcal mol^{-1}), as shown in Table 6. This indicated superior adsorption of molecule (**2**) compared to molecule (**1**). Additionally, the dE_{ads}/dN_i values for water molecules, hydronium ions, and Cl^- ions are approximately −18.17, −61.66, and −143.94 kcal mol^{-1}, respectively. These values were lower than those of (**1**) and (**2**) molecules, indicating strong adsorption of inhibitor molecules compared to water molecules, hydronium ions, and Cl^- ions. This improved the displacement of water molecules, hydronium ions, and chloride ions by inhibitor molecules. Therefore, molecules (**1**) and (**2**) were strongly adsorbed on the steel surface and formed a robust adsorbed shielding layer, providing corrosion inhibition for the steel interface in acid solutions. This has been confirmed by both empirical and theoretical investigations.

■ MATERIALS AND METHODS

Synthesis, Materials, and Equipment. The reagents were obtained from Sigma-Aldrich Company. ^{1}H- and ^{13}C-nuclear magnetic resonance (NMR) spectra were recorded on a JEOL spectrometer (JEOL, Tokyo, Japan) (400 or 500 MHz) in $CDCl_3$ and DMSO-d_6 and reported as chemical shifts (δ ppm). Infrared spectra were measured on a Thermo Scientific Nicolet iS10 FTIR spectrometer (Thermo Fisher Scientific, Waltham, MA). Elemental analyses were performed on a Perkin-Elmer 2400 elemental analyzer (PerkinElmer, Inc., Waltham, MA). High-resolution mass spectrometry (HRMS) was performed using a Bruker electrospray-ionisation quadrupole time-of-flight (ESI-QTOF) mass spectrometer (Bruker, Billerica, MA) in positive-ion mode.

The comprehensive methodology for all synthetic steps of morpholino-*s*-triazine derivatives has been documented by El-Faham et al.,[67] (Supporting Information S1).

Corrosion-Inhibition Experiment. *Weight Loss.* Carbon steel samples, with a dimension of 1.2 cm × 1.4 cm and thickness 0.05 cm, were immersed in 6 mL of HCl (1 M) in test tubes for 3 days without the addition of an inhibitor (blank tube) or with the addition of 1.25 mg of inhibitor (**1**) or inhibitor (**2**) in 0.25 mL of DMSO (inhibitor concentration = 200 ppm). The experiment was repeated for 7 days. At the end of each experiment, the samples were washed with distilled water, dried, and weighed.

Electrochemical Techniques. A three-electrode system was used for the anticorrosion study of the inhibitors. The working electrode consisted of a carbon-steel (C-steel) disc with an exposed area of 0.5027 cm^2, which was slightly less than the one used by other workers.[68−70] The C-steel disc was isolated with polytetrafluoroethylene and the exposed area was 0.5027 cm^2. The chemical composition of carbon steel rod was: % weight (wt %) C, 0.164; S, 0.001; Mn, 0.710; P, 0.0005; Si, 0.26, Ni, 0.123; Cr, 0.041; balance Fe. At the beginning of each experiment, the C-steel working electrode was buffed with a series of silicon carbide papers from 600 to 2000. The reference electrode was a saturated silver/silver chloride (Ag/AgCl) electrode, while the counter electrode was a platinum wire with length 3.6 cm and diameter 0.5 mm. The open-circuit potential, electrochemical impedance, and Tafel polarization were measured with a Gamry Instruments Reference 600 (potentiostat/galvanostat/ZRA) and computed using Gamry software v7.07. In a typical experiment, the sample was dissolved in 0.5 mL of DMSO, and then to it, 12 mL of HCl (1 M) was added in an aerated condition. The experiment was repeated twice. The open-circuit potential OCP was measured first for 1 h to ensure stabilization of the potential with time.

Computational Details. Theoretical calculations of these morpholine molecules as corrosion inhibitors were performed using density functional theory (DFT) with the B3LYP method with the 6-311++G(d,p) basis set implemented in the Gaussian 16W program package. Various quantum chemical descriptors are calculated to analyze the effectiveness of the corrosion inhibition properties. Total electronic energies, HOMO and LUMO orbital energies (E_{HOMO} and E_{LUMO}), and dipole moment (DM) values of the studied inhibitors were obtained from the optimization and frequency calculations. Other parameters such as the energy difference between the HOMO and LUMO (ΔE) of the inhibitors, their electron affinity (A), ionization potential (I), hardness (η), softness (S), electronegativity (χ), electronic chemical potential (μ), electrophilicity (ω), electron-donor capacity (ω^-), electron-acceptor capacity (ω^+), fractions of the electron transferred (ΔN), and back-donation ($\Delta E_{B\text{-}d}$) were calculated based on the HOMO and LUMO orbital analysis results. Additionally, Fukui indices were employed to evaluate the local relativity of the inhibitor.[71,72]

The I and A are associated with the E_{HOMO} and E_{LUMO} values, respectively, in the framework of Koopmans' theorem.[73]

$$I = -E_{HOMO} \tag{3}$$

$$A = -E_{LUMO} \tag{4}$$

The global reactivities (χ, μ, η, and S) can be measured from I and A[74] using the following equations

$$\chi = -\mu \frac{I + A}{2} \tag{5}$$

$$\eta = \frac{I - A}{2} \tag{6}$$

$$S = \frac{1}{\eta} \tag{7}$$

The electrophilicity (ω) was introduced by Parr et al.,[58] and it is a reactivity descriptor that measures the electron-accepting abilities.

It is defined as follows

$$\omega = \frac{\mu^2}{2} \tag{8}$$

The electron flow takes place from an inhibitor with lower electronegativity to a metallic surface with higher electro-

https://doi.org/10.1021/acsomega.4c02569
ACS Omega 2024, 9, 31714−31731

negativities to an extent where their chemical potential is the same.[75] Thus, the fraction of transferred electrons (ΔN) was estimated according to Pearson.[76]

$$\Delta N = \frac{\chi_{Fe} - \chi_{inh}}{2(\eta_{Fe} + \eta_{inh})} \quad (9)$$

From eq 7, the χ_{Fe} and χ_{inh} denote absolute electronegativity and the η_{Fe} and η_{inh} denote the absolute hardness of iron (Fe) and the inhibitor (inh) molecule, respectively. Theoretical values of χ_{Fe} = 7.0 eV mol^{-1} and η_{Fe} = 0 eV mol^{-1} are used upon the assumption that for a metallic bulk, $I = A$ because they are softer than the neutral metallic atoms.[77,78]

An electronic back-donation ($\Delta E_{B\text{-}d}$) arises from simple charge transfer between the inhibitor and the metal surface.[79] Assuming that charge transfer takes place from the inhibitor to the metal surface along with its converse process, ($\Delta E_{B\text{-}d}$) increases with decreasing η, as depicted below.

$$\Delta E_{B\text{-}d} = -\frac{\eta}{4} \quad (10)$$

Provided that $\eta > 0$ and $\Delta E_{B\text{-}d} < 0$ gives a clear indication that the charge transfer is energetically favorable.

The condensed Fukui function allows the identification of local selectivity within a corrosion inhibitor, through which the values describe the subjection of the atoms toward an electrophilic or nucleophilic attack.[80] The distinction between these nucleophilic and electrophilic Fukui functions can be derived from the given dual descriptor (Δf) equation.[81]

$$f_k^+ = q_{N+1} - q_N \quad \text{(for nucleophilic attack)} \quad (11)$$

$$f_k^- = q_N - q_{N-1} \quad \text{(for electrophilic attack)} \quad (12)$$

$$\Delta f = f_k^+ f_k^- \quad (13)$$

where q_N, q_{N+1}, and q_{N-1} are the electronic populations of the atom in neutral and protonated systems.

The site prefers a nucleophilic attack, given $\Delta f > 0$, while it is not prone to the attack, provided $\Delta f < 0$.

The local softness (s) of an atom can be calculated as follows

$$s^+ = (f_k^+)S \quad \text{(for nucleophilic attack)} \quad (14)$$

$$s^- = (f_k^-)S \quad \text{(for electrophilic attack)} \quad (15)$$

The calculated values explain the total molecular softness and thus are linked to the chemical reactivity. The higher s^+ indicates higher nucleophilicity, whereas the higher s^- indicates higher electrophilicity.

Monte Carlo (MC) Simulation Experiment. The adsorption positions of morpholine derivative (**1**) and (**2**) molecules on the Fe(110) surface were determined using the adsorption locator module in the Materials Studio V. 7.0 program[66] for MC simulations. The adsorbate molecules were initially optimized using the COMPASS force field.[82] The adsorption of inhibitors, Cl^- ions, hydronium ions, and water molecules on the Fe(110) surface was simulated in a box with dimensions of 37.24 Å × 37.24 Å × 59.81 Å.[83]

CONCLUSIONS

- The electrochemical results indicated that *s*-triazine/anilino-diazolo-morpholino derivatives (**1**) and bromine-substituted (**2**) showed excellent corrosion inhibition for C-steel in an HCl solution: 98.5% for inhibitor (**2**) at 80 ppm and 97.8% for inhibitor (**1**) at 100 ppm. Thus, a Br substituent enhanced inhibition.
- Tafel plots showed that the inhibition occurred by depressing the cathodic reactions.
- Compounds (**1**) and (**2**) exhibited Langmuir and Temkin isotherm adsorption, respectively, and the adsorption was spontaneous.
- SEM analysis indicated that the steel surface was smoother when the inhibitors were added to acidic media.
- The weight loss experiment indicated that the corrosion rate decreased when the inhibitors were used compared to the acid blank.
- E_{LUMO}, E_{HOMO}, and ΔE values conform to the experimental inhibition efficiencies. The inhibition efficiency increased with higher E_{HOMO}, lower E_{LUMO}, and smaller ΔE values.
- The value of the energy associated with the metal/adsorbate arrangement dE_{ads}/dN_i is higher for inhibitor (**2**) than for inhibitor (**1**), supporting the experimental results.

ASSOCIATED CONTENT

Data Availability Statement

All data are available in the main text or the electronic Supporting Information.

Supporting Information

The Supporting Information is available free of charge at https://pubs.acs.org/doi/10.1021/acsomega.4c02569.

Characterization of morpholino-*s*-triazine derivatives (S1), energies for neutral and protonated forms of morpho-*s*-triazine-H (**1**) and morpho-*s*-triazine-Br (**2**) calculated at the B3LYP/6-311++G(d,p) level of theory (Table S1); cartesian coordinates for neutral and protonated forms of (**1**) and (**2**) [B3LYP/6-311++G(d,p)] (Table S2); some chemical parameters for the neutral forms of (**1**) and (**2**) in the gaseous (g) phase calculated with the B3LYP method with the 6-311++G(d,p) basis set (Table S3); some chemical parameters for the protonated forms of (**1**) and (**2**) in the gaseous (g) phase calculated with the B3LYP method with the 6-311++G(d,p) basis set (Table S4); Mulliken atomic charges and electronic population for atoms of (**1**) and (**2**) in neutral and aqueous phases (Table S5); Mulliken atomic charges and electronic population for atoms of (**1**) and (**2**) in protonated and aqueous phases (Table S6); condensed Fukui indices, dual descriptors, and local softness for nucleophilic and electrophilic attacks for atoms of the neutral and protonated forms of inhibitors (**1**) and (**2**) in the aqueous phase (Table S7); FTIR spectra of inhibitors (**1**) and (**2**) (Figure S1), and effect of concentration on the open-circuit potential OCP of (a) (**1**) and (b) (**2**) in HCl (1 M) using C-steel (Figure S2) (PDF)

AUTHOR INFORMATION

Corresponding Authors

Hassan H. Hammud − *Department of Chemistry, College of Science, King Faisal University, Al-Ahsa 31982, Saudi Arabia*; Email: hhammoud@kfu.edu.sa

Nadeem S. Sheikh − *Chemical Sciences, Faculty of Science, Universiti Brunei Darussalam, Gadong BE1410, Brunei*

https://doi.org/10.1021/acsomega.4c02569
ACS Omega 2024, 9, 31714−31731

Darussalam; orcid.org/0000-0002-0716-7562; Email: nadeem.sheikh@ubd.edu.bn

Hany M. Abd El-Lateef − *Department of Chemistry, College of Science, King Faisal University, Al-Ahsa 31982, Saudi Arabia; Chemistry Department, Faculty of Science, Sohag University, Sohag 82524, Egypt;* orcid.org/0000-0002-6610-393X; Email: hmahmed@kfu.edu.sa

Authors

Waleed A. Aljamhi − *Department of Chemistry, College of Science, King Faisal University, Al-Ahsa 31982, Saudi Arabia*

Ihab Shawish − *Department of Math and Sciences, College of Humanities and Sciences, Prince Sultan University, Riyadh 11586, Saudi Arabia;* orcid.org/0000-0002-7988-7358

Nur Hazimah B. Z Arfan − *Chemical Sciences, Faculty of Science, Universiti Brunei Darussalam, Gadong BE1410, Brunei Darussalam*

Malai Haniti S. A. Hamid − *Chemical Sciences, Faculty of Science, Universiti Brunei Darussalam, Gadong BE1410, Brunei Darussalam*

Assem Barakat − *Department of Chemistry, College of Science, King Saud University, Riyadh 11451, Saudi Arabia;* orcid.org/0000-0002-7885-3201

Ayman El-Faham − *Chemistry Department, Faculty of Science, Alexandria University, Alexandria 21321, Egypt;* orcid.org/0000-0002-3951-2754

Complete contact information is available at: https://pubs.acs.org/10.1021/acsomega.4c02569

Author Contributions

H.H.H., N.S.S., and A.E.-F. conceptualized, designed, and supervised the project. H.H.H. acquired the funding for the project. I.S., N.B.B.Z.A., M.H.S.A.H., and A.B. contributed to the methodology and investigation. H.H.H. supervised the electrochemical investigation conducted by W.A.A. N.S.S. supervised the computational investigation conducted by N.B.B.Z.A. and M.H.S.A.H. All authors analyzed the results and got involved in writing the manuscript. H.H.H., N.S.S., and I.S. edited the manuscript to generate the final version of the manuscript, agreed by all of the authors.

Notes

The authors declare no competing financial interest.

Sample Availability The samples of novel synthesized compounds are available from the authors.

■ ACKNOWLEDGMENTS

This work was supported by the Deanship of Scientific Research, vice Presidency for Graduate Studies and Scientific Research, King Faisal University Saudi Arabia [Grant No. 3610]. The authors would like to acknowledge Prince Sultan University for their support.

■ REFERENCES

(1) Al-Sabagh, A. M.; Kandile, N. G.; Nasser, N. M.; Mishrif, M. R.; El-Tabey, A. E. Novel surfactants incorporated with 1,3,5-triethanolhexahydro-1,3,5-triazine moiety as corrosion inhibitors for carbon steel in hydrochloric acid: Electrochemical and quantum chemical investigations. *Egypt. J. Pet.* **2013**, *22*, 351−365.

(2) Ahamad, I.; Quraishi, M. A. Bis (benzimidazol-2-yl) disulphide: An efficient water-soluble inhibitor for corrosion of mild steel in acid media. *Corros. Sci.* **2009**, *51*, 2006−2013.

(3) Zhang, Q. B.; Hua, Y. X. Corrosion inhibition of mild steel by alkylimidazolium ionic liquids in hydrochloric acid. *Electrochim. Acta* **2009**, *54*, 1881−1887.

(4) Li, W.; He, Q.; Pei, C.; Hou, B. Experimental and theoretical investigation of the adsorption behaviour of new triazole derivatives as inhibitors for mild steel corrosion in acid media. *Electrochim. Acta* **2007**, *52*, 6386−6394.

(5) Solmaz, R.; Kardas, G.; Yazıcı, B.; Erbil, M. Inhibition Effect of Rhodanine for Corrosion of Mild Steel in Hydrochloric Acid Solution. *Prot. Met.* **2005**, *41*, 581−585.

(6) Kardas, G. The Inhibition effect of 2-thiobarbituric acid on the corrosion performance of mild steel in HCl solution. *Mater. Sci.* **2005**, *41*, 337−343.

(7) Quraishi, M. A.; Chauhan, D. S.; Saji, V. S. Heterocyclic Biomolecules as Green Corrosion Inhibitors. *J. Mol. Liq.* **2021**, *341*, No. 117265.

(8) Verma, C.; Rhee, K. Y.; Quraishi, M. A.; Ebenso, E. E. Pyridine Based N-Heterocyclic Compounds as Aqueous Phase Corrosion Inhibitors: A Review. *J. Taiwan Inst. Chem. Eng.* **2020**, *117* (2), 265−277.

(9) Verma, C.; Thakur, A.; Ganjoo, R.; Sharma, S.; Assad, H.; Kumar, A.; Quraishi, M. A.; Alfantazi, A. Coordination Bonding and Corrosion Inhibition Potential of Nitrogen-Rich Heterocycles: Azoles and Triazines as Specific Examples. *Coord. Chem. Rev.* **2023**, *488*, No. 215177.

(10) Singh, A. K.; Quraishi, M. A. Effect of Cefazolin on the corrosion of mild steel in HCl solution. *Corros. Sci.* **2010**, *52*, 152−160.

(11) Shukla, S. K.; Quraishi, M. A.; Prakash, R. A self-doped conducting polymer "polyanthranilic acid": An efficient corrosion inhibitor for mild steel in acidic solution. *Corros. Sci.* **2008**, *50*, 2867−2872.

(12) Quraishi, M. A.; Shukla, S. K. Poly(aniline-formaldehyde): A new and effective corrosion inhibitor for mild steel in hydrochloric acid. *Mater. Chem. Phys.* **2009**, *113*, 685−689.

(13) Al-Amiery, A. A.; Kadhum, H.; Alobaidy, A. H. M.; Mohamad, A. B.; Hoon, P. S. Novel Corrosion Inhibitor for Mild Steel in HCl. *Materials* **2014**, *7*, 662−672.

(14) Chauhan, D. S.; Quraishi, M. A.; Nik, W. B. W.; Srivastava, V. Triazines as a potential class of corrosion inhibitors: Present scenario, challenges and future perspectives. *J. Mol. Liq.* **2021**, *321*, No. 114747.

(15) Quraishi, M. A.; Chauhan, D. S.; Saji, V. S. *Heterocyclic Organic Corrosion Inhibitors: Principles and Applications*, 1st ed.; Elsevier Inc.: Amsterdam, 2020; p 298.

(16) Shukla, S. K.; Singh, A. K.; Ebenso, E. E. Pharmaceutically active compound as corrosion inhibitor for mild steel in acidic medium. *Int. J. Electrochem. Sci.* **2011**, *6*, 4276−4285.

(17) Chauhan, D. S.; Sorour, A. A.; Quraishi, M. A. An overview of expired drugs as novel corrosion inhibitors for metals and alloys. *Int. J. Pharm. Chem. Sci.* **2016**, *4*, 680−691.

(18) Xuehui, P.; Baorong, H.; Weihua, L.; Faqian, L.; Zhigang, Y. 2,3,5-Triphenyl-2H-tetrazolium chloride and 2,4,6-tri(2-pyridyl)-s-triazine on the corrosion of mild steel in HCl. *Chin. J. Chem. Eng.* **2007**, *15*, 909−915.

(19) Yoo, S. H.; Kim, Y. W.; Chung, K.; Kim, N. K.; Kim, J. S. Corrosion inhibition properties of triazine derivatives containing carboxylic acid and amine groups in 1.0 M HCl solution. *Ind. Eng. Chem. Res.* **2013**, *52*, 10880−10889.

(20) Abd El-Lateef, H. M.; Shalabi, K.; Arab, A. M.; Abdallah, Y. M. Corrosion Mitigation Performance of N80 Steel in 5% Sulfamic Acid Medium by Applying Novel Tetrahydro-1,2,4-triazines Including Triazene Moieties: Electrochemical and Theoretical Approaches. *ACS Omega* **2022**, *7*, 23380−23392.

(21) Nnaji, N. J.; Ujam, O. T.; Ibisi, N. E.; Ani, J. U.; Onuegbu, T. O.; Olasunkanmi, L. O.; Ebenso, E. E. Morpholine and Piperazine Based Carboxamide Derivatives as Corrosion Inhibitors of Mild Steel in HCl Medium. *J. Mol. Liq.* **2017**, *230*, 652−661.

(22) Fiorot, R. G.; Westphal, R.; Lemos, B. C.; Romagna, R. A.; Gonçalves, P. R.; Fernandes, M. R. N.; Ferreira, C.; Taranto, A. G.;

Greco, S. G. Synthesis Molecular Modelling and Anticancer Activities of New Molecular Hybrids Containing 1,4-Naphthoquinone, 7-Chloroquinoline, 1,3,5-Triazine and Morpholine Cores as PI3K and AMPK Inhibitors in the Metastatic Melanoma Cells. *J. Braz. Chem. Soc.* **2019**, *30*, 1860−1873.

(23) El-Mahdy, G. A.; Al-Rasheed, H. H.; Alshaikh, M.; Al-Lohedan, H. A.; El-Faham, A. 2,4-Dihydrazino-6-morpholino-1,3,5-Triaizne (DHMT) and 2,4-Dihydrazino-6-Piperidino-1,3,5-Triaizne (DHPT) as promising corrosion inhibitors of steel in acidic media. *Int. J. Electrochem. Sci.* **2016**, *11*, 5459−5472.

(24) Zhang, J.; Qiao, G.; Hu, S.; Yan, Y.; Ren, Z.; Yu, L. Theoretical evaluation of corrosion inhibition performance of imidazoline compounds with different hydrophilic groups. *Corros. Sci.* **2011**, *53*, 147−152.

(25) Becke, A. D. Perspective on Density functional thermochemistry. III. The role of exact exchange. *J. Chem. Phys.* **1993**, *98*, 1372−1377.

(26) Masoud, M. S.; Awad, M. K.; Shaker, M. A.; El-Tahawy, M. M. T. The role of structural chemistry in the inhibitive performance of some aminopyrimidines on the corrosion of steel. *Corros. Sci.* **2010**, *52*, 2387−2396.

(27) Zarrouk, A.; Hammouti, B.; Dafali, A.; Bouachrine, M.; Zarrok, H.; Boukhris, S.; Al-Deyab, S. S. A theoretical study on the inhibition efficiencies of some quinoxalines as corrosion inhibitors of copper in nitric acid. *J. Saudi Chem. Soc.* **2014**, *18*, 450−455.

(28) Shawish, I.; Barakat, A.; Aldalbahi, A.; Malebari, A. M.; Nafie, M. S.; Bekhit, A. A.; Albohy, A.; Khan, A.; Ul-Haq, Z.; Haukka, M.; de la Tore, B. G.; Albericio, F.; El-Faham, A. Synthesis and Antiproliferative Activity of a New Series of Mono- 2 and Bis(dimethylpyrazolyl) - s - triazine Derivatives Targeting EGFR/ 3 PI3K/AKT/mTOR Signaling Cascades. *ACS Omega* **2022**, *7*, 24858−24870.

(29) Chen, Y.; Chen, Z.; Zhuo, Y. Newly synthesized morpholinyl Mannich Bases as corrosion inhibitors for N80 steel in acid environment. *Materials* **2022**, *15*, No. 4218.

(30) Xiong, L.; Wang, P.; He, Z.; Chen, Q.; Pu, J.; Zhang, R. Corrosion behaviors of Q235 carbon steel under imidazoline derivatives as corrosion inhibitors: Experimental and computational investigations. *Arab. J. Chem.* **2021**, *14* (2), No. 102952.

(31) Ituen, E.; Akaranta, O.; James, A. Electrochemical and anticorrosion properties of 5-hydroxytryptophan on mild steel in a simulated well-acidizing fluid. *J. Taibah Univ. Sci.* **2017**, *11*, 788−800.

(32) Lei, X.; Wang, H.; Feng, Y.; Zhang, J.; Sun, X.; Lai, S.; Wang, Z.; Kang, S. Synthesis, evaluation and thermodynamics of a 1H-benzoimidazole phenanthroline derivative as a novel inhibitor for mild steel against acidic corrosion. *RSC Adv.* **2015**, *5*, 99084−99094.

(33) Mikhaylichenko, S. N.; Patel, S. M.; Dalili, S.; Chesnyuk, A. A.; Zaplishny, V. N. Synthesis and structure of new 1,3,5-triazine-pyrazole derivatives. *Tetrahedron Lett.* **2009**, *50*, 2505−2508.

(34) El-Hajjaji, F.; Messali, M.; Aljuhani, A.; Aouad, M. R.; Hammouti, B.; Belghiti, M. E.; Chauhan, D. S.; Quraishi, M. A. Pyridazinium-based ionic liquids as novel and green corrosion inhibitors of carbon steel in acid medium: Electrochemical and molecular dynamics simulation studies. *J. Mol. Liq.* **2018**, *249*, 997−1008.

(35) Al Otaibi, N.; Hammud, H. H. Corrosion Inhibition Using Harmal Leaf Extract as an Eco-Friendly Corrosion Inhibitor. *Molecules* **2021**, *26* (22), No. 7024.

(36) Verma, C.; Olasunkanmi, L. O.; Ebenso, E. E.; Qurashi, M. A. Substituents effect on corrosion inhibition performance of organic compounds in aggressive ionic solutions: A review. *J. Mol. Liq.* **2018**, *251*, 100−118.

(37) Verma, C.; Alfantazi, A.; Quraishi, M. A.; Rhee, K. Y. Significance of Hammett and Taft substituent constants on bonding potential of organic corrosion inhibitors: Tailoring of reactivity and performance. *Coord. Chem. Rev.* **2023**, *495*, No. 215385.

(38) Hammud, H. H.; Maache, S. A.; Al-Otaibi, N.; Sheikh, N. S. An integrated experimental and theoretical studies on the inhibition of carbon steel by harmal extracts. *Molecules* **2022**, *27*, No. 7250.

(39) Sajadi, G. S.; Naghizade, R.; Zeidabadinejad, L.; Golshani, Z.; Amiri, M.; Hosseini, S. M. A. Experimental and theoretical investigation of mild steel corrosion control in acidic solution by Ranunculus arvensis and Glycine max extracts as novel green inhibitors. *Heliyon* **2022**, *8*, No. e10983.

(40) Douche, D.; Elmsellem, H.; Anouar, E. H.; Guo, L.; Hafez, B.; Tuzun, B.; Louzi, A. E.; Bougrin, K.; Karrouchi, K.; Himmi, B. Anti-corrosion performance of 8-hydroxyquinoline derivatives for mild steel in acidic medium: Gravimetric, electrochemical, DFT and molecular dynamics simulation investigations. *J. Mol. Liq.* **2020**, *308*, No. 113042.

(41) Kokalj, A. On the use of the Langmuir and other adsorption isotherms in corrosion Inhibition. *Corros. Sci.* **2023**, *217*, No. 111112.

(42) Ali, A. I.; Mahrous, Y. S. Corrosion inhibition of C-steel in acidic media from fruiting bodies of Melia azedarach L. extract and a synergistic Ni^{2+} additive. *RSC Adv.* **2017**, *7*, 23687−23698.

(43) Ward, T. M.; Weber, J. B. Aqueous solubility of alkylamino-s-triazine as a function of pH and molecular structure. *J. Agric. Food Chem.* **1968**, *16* (6), 959−961.

(44) Yoo, S.-H.; Kim, Y.-W.; Chung, K.; Kim, N.-K.; KIM, J.-S. Corrosion inhibition properties of triazine derivatives containing carboxylic acid and amine groups in 1.0 M HCl solution. *Ind. Eng. Chem. Res.* **2013**, *52*, 10880−10889.

(45) Shukla, S. K.; Singh, A. K.; Quraishi, M. A. Triazines: Efficient Corrosion Inhibitors for Mild Steel in Hydrochloric Acid Solution. *Int. J. Electrochem. Sci.* **2012**, *7*, 3371−3389.

(46) Yoo, S.-H.; Kim, Y.-W.; Shin, J.; Kim, N.-K.; Kim, J.-S. Effects of the Chain Length of Tris(carboxyalkylamino)triazine on Corrosion Inhibition Properties. *Bull. Korean Chem. Soc.* **2015**, *36*, 346−355.

(47) Obot, I.; Umoren, S.; Gasem, Z.; Suleiman, R.; Ali, B. E. Theoretical prediction and electrochemical evaluation of vinylimidazole and allylimidazole as corrosion inhibitors for mild steel in 1 M HCl. *J. Ind. Eng. Chem.* **2015**, *21*, 1328−1339.

(48) Xu, B.; Ji, Y.; Zhang, X.; Jin, X.; Yang, W.; Chen, Y. Experimental and theoretical studies on the corrosion inhibition performance of 4-amino-N, N-di-(2-pyridylmethyl)-aniline on mild steel in hydrochloric acid. *RSC Adv.* **2015**, *5*, 56049−56059.

(49) Hemmelmann, J. C.; Xu, H.; Krumm, W. Empirical Modeling of Iron Oxide Dissolution in Sulphuric and Hydrochloric Acid. *Metall. Mater. Trans. B* **2013**, *44* (5), 1232−1235.

(50) Kim, Y.-S.; Kim, J.-G. Corrosion Behavior of Pipeline Carbon Steel under Different Iron Oxide Deposits in the District Heating System. *Metals* **2017**, *7* (5), No. 182, DOI: 10.3390/met7050182.

(51) Govindarajan, M.; Karabacak, M. FT-IR, FT-Raman and UV spectral investigation; computed frequency estimation analysis and electronic structure calculations on 1-nitronaphthalene. *Spectrochim. Acta, Part A* **2012**, *85* (1), 251−260.

(52) Chakraborty, T.; Gazi, K.; Ghosh, D. C. Computation of the atomic radii through the conjoint action of the effective nuclear charge and the ionization energy. *Mol. Phys.* **2010**, *108*, 2081−2092.

(53) Obot, I. B.; Obi-Egbedi, N. O.; Umoren, S. A. Antifungal drugs as corrosion inhibitors for aluminium in 0.1 M HCl. *Corros. Sci.* **2009**, *51*, 1868−1875.

(54) Tang, Y. M.; Chen, Y.; Yang, W. Z.; Liu, W.; Yin, Z. S.; Wang, J. T. Electrochemical and theoretical studies of thienyl-substituted amino triazoles on corrosion inhibition of copper in 0.5 M H_2SO_4. *J. Appl. Electrochem.* **2008**, *38*, 1553−1559.

(55) Obot, I. B.; Macfonald, D. D.; Gasem, Z. M. Density functional theory (DFT) as a powerful tool for designing new organic corrosion inhibitors. Part 1: An overview. *Corros. Sci.* **2015**, *99*, 1−30.

(56) Kayadibi, F.; Sagdinc, S. G.; Kara, Y. S. Density functional theory studies on the corrosion inhibition of benzoin, benzil, benzoin-(4-phenylthiosemicarbazone) and benzil-(4-phenylthiosemicarbazone) of mild steel in hydrochloric acid. *Prot. Met. Phys. Chem. Surf.* **2015**, *51*, 143−154.

(57) Lukovits, I.; Kalman, E.; Zucchi, F. Experimental and quantum investigations of novel corrosion inhibitors based triazene derivatives for mild steel. *Corrosion* **2001**, *57*, 3−8.

(58) Parr, R. G.; Szentpaly, L. V.; Liu, S. Electrophilicity Index. *J. Am. Chem. Soc.* **1999**, *121*, 1922−1924.
(59) Abdelsalam, M. M.; Bedair, M. A.; Hassan, A. M.; Heakal, B. H.; Younis, A.; Elbialy, Z. I.; Badawy, M. A.; Fawzy, H. E. D.; Fareed, S. A. Green synthesis, electrochemical, and DFT studies on the corrosion inhibition of steel by some novel triazole Schiff base derivatives in hydrochloric acid solution. *Arab. J. Chem.* **2022**, *15*, No. 103491.
(60) Udhayakala, P.; Samuel, A. M.; Rajendiran, T. V.; Gunasekaran, S. DFT study on the adsorption mechanism of some phenyltetrazole substituted compounds as effective corrosion inhibitors for mild steel. *Pharma Chem.* **2013**, *5*, 111−124.
(61) Abd El-Lateef, H. M.; Shalabi, K.; Sayed, A. R.; Gomha, S. M.; Bakir, E. M. The novel polythiadiazole polymer and its composite with α-$Al(OH)_3$ as inhibitors for steel alloy corrosion in molar H_2SO_4: Experimental and computational evaluations. *J. Ind. Eng. Chem.* **2022**, *105*, 238−250.
(62) El-Mokadem, T. H.; Hashem, A. I.; Abd El-Sattar, N. E. A.; Dawood, E. A.; Abdelshafi, N. S. Green synthesis, electrochemical, DFT studies and MD simulation of novel synthesized thiourea derivatives on carbon steel corrosion inhibition in 1.0 M HCl. *J. Mol. Struct.* **2023**, *1274*, No. 134567.
(63) Abdelshafi, N. S.; Ibrahim, M. A.; Badran, A. S.; Halim, S. A. Experimental and theoretical evaluation of a newly synthesized quinoline derivative as corrosion inhibitor for iron in 1.0 M hydrochloric acid solution. *J. Mol. Struct.* **2022**, *1250*, No. 131750.
(64) Shalabi, K.; Helmy, A. M.; El-Askalany, A. H.; Shahba, M. M. New pyridinium bromide mono-cationic surfactant as corrosion inhibitor for carbon steel during chemical cleaning: Experimental and theoretical studies. *J. Mol. Liq.* **2019**, *293*, No. 111480.
(65) Özcan, M.; Dehri, I.; Erbil, M. Organic sulphur-containing compounds as corrosion inhibitors for mild steel in acidic media: correlation between inhibition efficiency and chemical structure. *Appl. Surf. Sci.* **2004**, *236*, 155−164.
(66) Dehghani, A.; Mostafatabar, A. H.; Bahlakeh, G.; Ramezanzadeh, B. A detailed study on the synergistic corrosion inhibition impact of the Quercetin molecules and trivalent europium salt on mild steel; electrochemical/surface studies, DFT modeling, and MC/MD computer simulation. *J. Mol. Liq.* **2020**, *316*, No. 113914.
(67) Sharma, A.; Ghabour, H.; Khan, S. T.; de la Tore, B. G.; Albericio, F.; El-Faham, A. Novel pyrazolyl-s-triazine derivatives, molecular structure and antimicrobial activity. *J. Mol. Struct.* **2017**, *1145*, 244−253.
(68) Jafari, H.; Danaee, I.; Eskandari, H.; RashvandAvei, M. Combined Computational and Experimental Study on the Adsorption and Inhibition Effects of N_2O_2 Schiff Base on the Corrosion of API 5L Grade B Steel in 1mol/L HCl. *J. Mater. Sci. Technol.* **2014**, *30* (3), 239−252.
(69) Jafari, H.; Danaee, I.; Eskandari, H.; Rashvandavei, M. Electrochemical and Theoretical Studies of Adsorption and Corrosion Inhibition of N,N'-Bis(2-Hydroxyethoxyacetophenone)-2,2-Dimethyl-1,2- Propanediimine on Low Carbon Steel (API 5L Grade B) in Acidic Solution. *Ind. Eng. Chem. Res.* **2013**, *52* (20), 6617−6632.
(70) Jafari, H.; Ameri, E.; Vakili, M. H.; Berisha, A. Novel Silicon-based schiff-base as corrosion inhibitor for anti-corrosion behavior of API 5L Grade B in 1M HCl. *Mater. Chem. Phys.* **2024**, *311*, No. 128499.
(71) Yang, W.; Mortier, W. J. The use of global and local molecular parameters for the analysis of the gas-phase basicity of amines. *J. Am. Chem. Soc.* **1986**, *108*, 5708−5711.
(72) Rodriguez-Valdez, L. M.; Martinez-Villafane, A.; Glossman-Mitnik, D. Computational simulation the molecular structure and properties of heterocyclic organic compounds with possible corrosion inhibition properties. *J. Mol. Struct.: THEOCHEM* **2005**, *713*, 65−70.
(73) Koopmans, T. The use of global and local molecular parameters for the analysis of the gas-phase basicity of amines. *Physica* **1934**, *41*, No. 104.
(74) Lesar, A.; Milošev, I. Density functional study of the corrosion inhibition properties of 1,2,4-triazole and its amino derivatives. *Chem. Phys. Lett.* **2009**, *483*, 198−203.
(75) Martinez, S. Inhibitory mechanism of mimosa tannin using molecular modeling and substitutional adsorption isotherms. *Mater. Chem. Phys.* **2003**, *77*, 97−102.
(76) Pearson, R. G. Absolute electronegativity and hardness: application to inorganic chemistry. *Inorg. Chem.* **1988**, *27*, 734−740.
(77) Sastri, V. S.; Perumareddi, J. R. Molecular Orbital Theoretical Studies of Some Organic Corrosion Inhibitors. *Corrosion* **1997**, *53*, 617−622.
(78) Lukovits, I.; Kalman, E.; Zucchi, F. Corrosion Inhibitors—Correlation between Electronic Structure and Efficiency. *Corrosion* **2001**, *57*, 3−8.
(79) Gómez, B.; Likhanova, N. V.; Dominguez-Aguilar, M. A.; Martinez-Pulou, R.; Vela, A.; Gazquez, J. L. Quantum Chemical Study of the Inhibitive Properties of 2-Pyridyl-Azoles. *J. Phys. Chem. B* **2006**, *110*, 8928−8934.
(80) Fuentealba, P.; Perez, P.; Contreras, R. On the condensed Fukui function. *J. Chem. Phys.* **2000**, *113*, 2544−2551.
(81) Morell, C.; Grand, A.; Toro-Labbe, A. New Dual Descriptor for Chemical Reactivity. *J. Phys. Chem. A* **2005**, *109*, 205−212.
(82) Feng, Y.; Chen, S.; Guo, W.; Zhang, Y.; Liu, G. Inhibition of iron corrosion by 5,10,15,20-tetraphenylporphyrin and 5,10,15,20-tetra-(4-chlorophenyl)porphyrin adlayers in 0.5 M H_2SO_4 solutions. *J. Electroanal. Chem.* **2007**, *602*, 115−122.
(83) Abd El-Lateef, H. M.; Shalabi, K.; Tantawy, A. H. Corrosion inhibition and adsorption features of novel bioactive cationic surfactants bearing benzenesulphonamide on C1018-steel under sweet conditions: Combined modeling and experimental approaches. *J. Mol. Liq.* **2020**, *320*, No. 114564.

https://doi.org/10.1021/acsomega.4c02569
ACS Omega 2024, 9, 31714−31731